Nucleic Acids Research, 2025, **53**, gkaf174
https://doi.org/10.1093/nar/gkaf174
Gene regulation, Chromatin and Epigenetics

Transcription factor VIB-1 activates *catalase-3* expression by promoting PIC assembly in *Neurospora crassa*

Huan Liu[1,†], Qin Zhang[1,†], Fusheng Huang[1], Shuangjie Shen[1], Moater Altaf[1], Ying Wang[1], Xiao Liu[2,3,*], Qun He[1,*]

[1]MOA Key Laboratory of Soil Microbiology, College of Biological Sciences, China Agricultural University, Beijing100193, China
[2]State Key Laboratory of Mycology, Institute of Microbiology, Chinese Academy of Sciences, Beijing100101, China
[3]College of Life Sciences, University of the Chinese Academy of Sciences, Beijing100049, China

[*]To whom correspondence should be addressed. Email: qunhe@cau.edu.cn
Correspondence may also be addressed to Xiao Liu. Email: liux@im.ac.cn
[†]These authors contributed equally to this work.

Abstract

The "p53-like" superfamily transcription factor, VIB-1, plays a crucial role in mediating heterokaryon incompatibility and regulating the transcription of specific genes involved in the secretion of extracellular hydrolases in *Neurospora crassa*. However, the precise mechanism underlying the transcriptional regulatory function of VIB-1 is still poorly understood. Here, we reveal that VIB-1 is involved in the H_2O_2-induced oxidative stress response, in which deletion of *vib-1* leads to an H_2O_2-sensitive phenotype and inhibition of *cat-3* expression. Conversely, VIB-1 overexpression confers an H_2O_2-resistant phenotype and robustly activates *cat-3* in a dose-dependent manner. Importantly, we identified the DNA-binding domain of VIB-1 as the key component required for these regulatory processes. Furthermore, VIB-1 activates *cat-3* transcription by interacting with and recruiting general transcription factors and RNA polymerase II to the *cat-3* promoter, resulting in eviction of H2A.Z and a decrease in nucleosome density in these regions. Additionally, VIB-1 positively regulated the expression of other two target genes, NCU05841 and NCU02904, in the same manner. Together, our findings reveal a mechanism by which VIB-1 is involved in the transcriptional activation of *cat-3* and other VIB-1-targeted genes by promoting PIC assembly on their promoters.

Graphical abstract

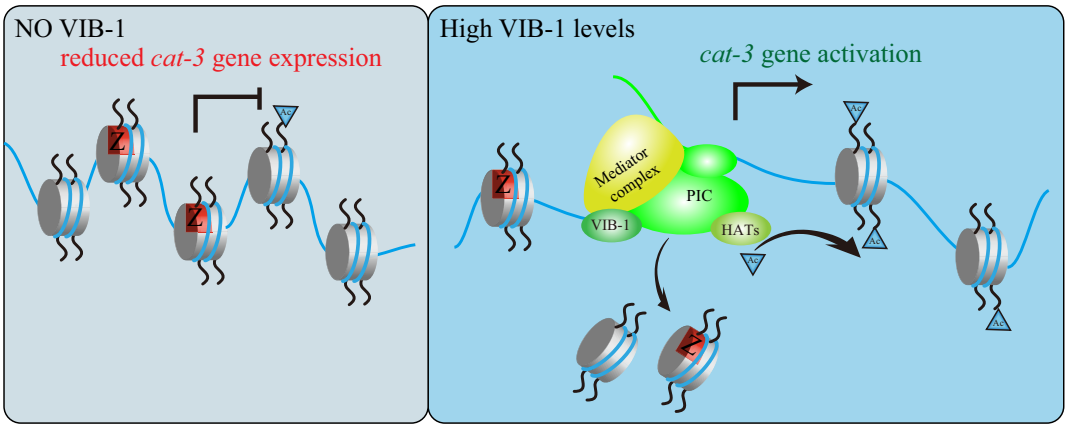

Introduction

Reactive oxygen species (ROS), which are produced by aerobic organisms through the electron transport chain during endogenous and extracellular redox reactions, ubiquitously involved in the regulation of diverse cellular functions, such as governing cell-cycle phase transitions, serving as intracellular signaling molecules in signal transduction pathways during normal metabolism, or being stimulated by an external environment [1, 2]. Biochemically, ROS are a heterogeneous group of highly reactive ions and molecules derived from oxygen, specifically composed of superoxide anion, hydrogen peroxide (H_2O_2), hydroxyl radicals, and singlet oxygen, which impart unique chemical properties to various biological macromolecules in living organisms [3]. Elevated ROS levels beyond homeostasis have detrimental effects on living organisms, including damage to biological macromolecules such as nucleic

Received: September 3, 2024. **Revised:** February 7, 2025. **Editorial Decision:** February 20, 2025. **Accepted:** February 22, 2025

acids, proteins, and lipids, and even cell death in serious cases [4–6]. Therefore, the timely removal of excess ROS and the maintenance of intracellular ROS homeostasis are essential for the survival and development of living organisms. Enzymatic antioxidants, such as superoxide dismutase, catalase, peroxiredoxin, glutathione peroxidase, and glutathione peroxidase play a crucial role in the removal of ROS [7, 8].

Catalases (CATs) are necessary for the conversion of H_2O_2 to dioxygen and water, and are highly conserved and precisely regulated at multiple levels to achieve redox homeostasis in aerobionts [8–11]. Thus, catalase plays an important role in eliminating excess ROS and maintaining intracellular ROS homeostasis at different stages of development. There are three catalases, CAT-1, CAT-3, and CAT-4, and one catalase-peroxidase, CAT-2, which are expressed in *Neurospora crassa* at different stages of its asexual life cycle [12, 13]. Consistent with the ROS levels in different cells, CAT-1 mainly accumulates in conidia, while CAT-2 is generally produced in both aerial hyphae and conidia. CAT-3 plays a dominant role in the active mycelia and in the early stages of conidia formation. Importantly, the antioxidant function of CAT-3 cannot be replaced by other catalases [12, 14]. CAT-3 is a catalase that can also be induced by different stress conditions, such as exogenous hydrogen peroxide, paraquat, $CaCO_3$, uric acid, and heat shock [12]. Our previous work has identified several transcriptional regulators of *cat-3* transcription. For example, CPC-1 (Cross-Pathway Control-1, homologous to General Control Non-derepressible 4 (GCN4) in *Saccharomyces cerevisiae*), coordinates with the histone acetyltransferase NGF-1 (Neurospora GCN5 Factor-1, homologous to General Control Non-derepressible 5 (GCN5)) to positively regulate *cat-3* expression in response to H_2O_2-induced oxidative stress [15]. Conversely, the histone variant H2A.Z negatively regulates the transcription of *cat-3*. SWR complex-mediated H2A.Z deposition and NC2α/β-INO80C-mediated H2A.Z removal from the transcription start site (TSS) of the *cat-3* locus both significantly influence *cat-3* transcription [16, 17]. We also found that Bub3/Ada21 represses *cat-3* transcription by maintaining BuGZ binding to *cat-3*, and deletion of BuGZ leads to increased recruitment of CPC-1 and NC2α/β to regulatory regions of *cat-3* [18]. By contrast, we found that deletion of histone deacetylase HDA-2 (Histone Deacetylase-2) and its partner proteins results in decreased expression of *cat-3*, elevated acetylation levels of histone H4, and high deposition of H2A.Z at the *cat-3* locus [19]. These results indicate that chromatin structure and histone modifications play major roles in regulating the inducible expression of the *cat-3*. However, it is unclear how these transcription factors and chromatin regulators are organized to control *cat-3* expression, and it is not known whether other transcriptional regulators are involved in the regulation of *cat-3* expression by affecting chromatin structure and histone modification during physiological conditions.

In fungi, Ndt80-like transcription factors, belonging to the "p53-like" superfamily, play crucial roles in regulating various processes. These include regulation of efflux pumps [20, 21], GlcNAc sensing/metabolism [22], sexual reproduction [23], hyphal growth and virulence, regulation of pigment production [24, 25], and protease production [26, 27]. Similar to the p53 protein, the Ndt80-like transcription factor functions as a general starvation response transcription factor that is important for the basal expression of nutrient acquisition genes. Three Ndt80 homolog proteins—VIB-1 (Vegetative Incompatibility Block-1, NCU03725), FSD-1 (Female Sexual Development-1, NCU09915), and RON-1 (Regulator of N-Acetylglucosamine, NCU04729)—were found in *N. crassa* [23, 28]. VIB-1 regulates heterokaryon incompatibility (HI) by controlling the expression of heterokaryon-incompatible related genes at the mating-type or *het-c* loci, which causes programmed cell death (PCD) in heterokaryon [29, 30]. Unlike in *Saccharomyces cerevisiae*, none of the three members are necessary for the meiosis process in *N. crassa*, while genetic analysis has shown that FSD-1 and VIB-1 regulate the formation of female reproductive structures (protoperithecia) [23, 31, 32]. VIB-1 is required for extracellular protease production in response to nitrogen and carbon starvation [33], and for the utilization of cellulose by affecting the expression levels of CLR2, an important regulator of the hydrolase gene [34, 35]. Interestingly, constitutive expression of *Trichoderma reesei vib-1* in a *N. crassa vib-1* mutant can fully restore growth and cellulolytic enzyme activity, where TrVIB-1 and *N. crassa* VIB-1 share 49% amino acid identity [34]. Together, these observations suggest a general role for VIB-1 homologs in sensing and responding to environmental nutrients to determine which sets of genes to activate. On the other hand, starvation increases the frequency of vegetative cell fusion in several ascomycete fungi [36–38]. ROS levels increase during mycelial fusion in *N. crassa*. As an important transcription factor for nutrient sensing and cell fusion, VIB-1 regulates the transcription of nutrient acquisition genes and HET domain genes. However, the molecular mechanism by which VIB-1 regulates the expression of target genes is unclear.

Here, we found that the transcription factor VIB-1 activates *cat-3* expression in a dose-dependent manner, depending on its DNA-binding domain. Chromatin immunoprecipitation (ChIP) assays revealed that VIB-1 binds to the promoter region of *cat-3* and regulates its expression by promoting the assembly of the transcription preinitiation complex (PIC) through interactions with general transcription factors (GTFs), resulting in altered chromatin structure. Collectively, our work elucidates the underlying mechanism by which VIB-1 functions in transcriptional regulation.

Materials and methods

Strains and culture conditions

In this study, *87–3* (*bd, a*) [39] was used as the wild-type (WT) strain. The *ku70*^{RIP} (*bd, a*) strain [40], generated previously, was used as the host strain for creating the *vib-1*^{KO} strain. The *H2A.Z*^{KO} strain [16], *cat-3*^{KO} strain [41], *Nc2α*^{KO} strain [17], *cpc-1* (j-5) strain [15], and *upf-3*^{KO} [42], generated previously, were also used in this study. The *vib-1*^{KO};*H2A.Z*^{KO} or *upf-3*^{KO};*vib-1*^{KO}strain was generated by crossing *vib-1*^{KO} with *H2A.Z*^{KO} or *upf-3*^{KO}. The *vib-1*^{KO};Myc-VIB-1, *vib-1*^{KO};Myc-VIB-1^{R190AR191A}, *vib-1*^{KO};Myc-VIB-1^{R290AR291A}, *vib-1*^{KO};Myc-VIB-1$^{\triangle DBD}$, *wt*;Myc-VIB-1, *wt*;Myc-VIB-1^{R190AR191A}, *wt*;Myc-VIB-1^{R290AR291A}, or *wt*;Myc-VIB-1$^{\triangle DBD}$ strains were generated by transferring *pcfp*-Myc-VIB-1, *pcfp*-Myc-VIB-1^{R190AR191A}, *pcfp*-Myc-VIB-1^{R290AR291A}, and *pcfp*-Myc-VIB-1$^{\triangle DBD}$ constructs into the *his-3* locus of *vib-1*^{KO} (*his-3, A*) or the *301–6* (*his-3, A*) strain. The *Nc2α*^{KO};Myc-VIB-1 strain was generated by transferring *pcfp*-Myc-VIB-1 into the *his-3* locus of the *Nc2α*^{KO} strain (*his-3, A*). The *cpc-1* (j-5);Myc-VIB-1 strain was generated by transferring *pcfp*-Myc-VIB-1 into

the *cpc-1* (j-5) strain genomic DNA with the NrsR [43] as the resistance screening gene. The *wt*;Myc-MED-1, *wt*;Myc-MED-4, *wt*;Myc-MED-5, *wt*;Myc-MED-8, *wt*;Myc-MED-10, *wt*;Myc-MED-12, *wt*;Myc-MED-14, *wt*;Myc-MED-16, *wt*;Myc-MED-17, *wt*;Myc-MED-18, and *wt*;Myc-TFIIB strains were generated by transferring *pcfp*-Myc-MED-1, *pcfp*-Myc-MED-4, *pcfp*-Myc-MED-5, *pcfp*-Myc-MED-8, *pcfp*-Myc-MED-10, *pcfp*-Myc-MED-12, *pcfp*-Myc-MED-14, *pcfp*-Myc-MED-16, *pcfp*-Myc-MED-17, *pcfp*-Myc-MED-18, and *pcfp*-Myc-TFIIB constructs into the *301–6* strain (*his-3, A*), respectively. The *vib-1*^{KO};Myc-MED-16 and *vib-1*^{KO};Myc-MED-17 strains were generated by transferring *pcfp*-Myc-MED-16 and *pcfp*-Myc-MED-17 constructs into the *vib-1*^{KO} strain (*his-3, A*), respectively. The *vib-1*^{KO};HA-VIB-1^{WT}, *vib-1*^{KO};HA-VIB-1$^{\triangle AD1}$, *vib-1*^{KO};HA-VIB-1$^{\triangle AD2}$, *vib-1*^{KO};HA-VIB-1$^{\triangle AD3}$, and *vib-1*^{KO};HA-VIB-1$^{\triangle AD}$ strains were generated by transferring *pcfp*-HA-VIB-1^{WT}, *pcfp*-HA-VIB-1$^{\triangle AD1}$, *pcfp*-HA-VIB-1$^{\triangle AD2}$, *pcfp*-HA-VIB-1$^{\triangle AD3}$, and *pcfp*-HA-VIB-1$^{\triangle AD}$ constructs into the *his-3* locus of *vib-1*^{KO} (*his-3, A*) strain, respectively. All strains constructed in this study possess a *band* background.

Conidia of the indicated strains were inoculated in petri dishes with 50 ml of minimal medium (1× Vogel's and 2% glucose) and cultured at 25°C in constant light until the exponential growth phase of the mycelia. The mycelial mats were cut with a specific puncher for quantification. Then, these small mycelial disks were transferred to Erlenmeyer flasks with 50 ml minimal medium and were grown at 25°C with shaking for 18 h under constant light.

Plate assay

The medium for plate assays contained 1× Vogel's, 3% sucrose, and 1.5% (w/v) agar with different concentrations of H_2O_2. WT or mutant strains were inoculated at the center of the disks and grown under constant light at 25°C on the medium. When the WT strain almost completely covered the medium without H_2O_2, all the plates were scanned, and the average growth rate of each strain relative to that in the medium without H_2O_2 (0 mM) was calculated. The growth diameter of WT and mutants under 0 mM H_2O_2 was defined as their respective reference unit "1," and the relative growth of WT and mutants under other different concentrations of H_2O_2 was calculated, respectively. Each experiment was performed at least three times independently [17].

Generation of antiserum against VIB-1

The GST-VIB-1 (amino acids Pro439-Thr639) fusion protein was expressed in *Escherichia coli* BL21 cells, and the soluble recombinant protein was purified and used as the antigen to generate rabbit polyclonal antiserum as described previously [44].

In-gel assay for catalase activities

Sample preparation, protein extraction, and quantification for the in-gel assay were the same as previously described [41, 45]. Equal amounts of total protein (25 μg) were loaded into each protein lane of a 7.5% native polyacrylamide gel. After 3 h of electrophoresis, the gel was soaked in 7 mM H_2O_2 with gentle shaking for 10 min, and then immediately transferred into a freshly prepared mixture containing 1% potassium hexacyanoferrate (III) and 1% iron (III) chloride hexahydrate. Catalase activities were visualized as bright bands where H_2O_2 was decomposed by catalases.

The stained colonies for testing extracellular catalase activity

A small amount of 7-day-old conidia was resuspended in 1 ml of ddH_2O, and 0.2 μl of this conidial suspension was incubated on solid medium containing 1× Vogel's, 1.5% agar, and 1× Fig's at 30 °C for 4 days. Similar to the In-gel assay for catalase activities [45], the medium with colonies in Petri dishes was treated with 7 mM H_2O_2 for 10 min, then washed with ddH_2O and immersed in a mixture of freshly prepared 1% potassium hexacyanoferrate (III) and 1% iron (III) chloride hexahydrate for 2 min. Extracellular catalases were visualized as a transparent circle (halo) where H_2O_2 was decomposed by the catalases.

Protein analyses

Protein extraction, quantification, and western blot analysis were performed as described previously [44]. Equal amounts of total protein (32 μg) were loaded into each protein lane of an SDS–polyacrylamide gel and separated by electrophoresis. Then, the total proteins were transferred onto a PVDF (Polyvinylidene Fluoride) membrane and western blot analysis was performed using an antibody against the target protein.

RT-qPCR (Reverse Transcription Quantitative Polymerase Chain Reaction)

Total RNA was extracted with TRIzol reagent and each RNA sample (5 μg) was subjected to reverse transcription with a commercial reverse transcription kit (Thermo Scientific, #M1682), and the cDNA was amplified by qPCR. The primers used for qPCR are shown in Supplementary Table S1. The relative value of gene expression was calculated using the $2^{-\Delta\Delta CT}$ method [46] by comparing the cycle numbers for each sample to those for the untreated control. The results were normalized to the expression levels of the *β-tubulin* gene [15, 17].

Coimmunoprecipitation assays

Cell extracts from the conidia incubated for 24 h were used to perform protein coimmunoprecipitation analyses. Protein extraction, quantification, and coimmunoprecipitation assays were performed as described previously [17]. Briefly, 3 mg/ml protein extracts in extraction buffer were incubated with 3 μl of monoclonal antibody against c-Myc (HT101-02, TransGen Biotech) for 4 h at 4°C with rotation. Then, the 40 μl of precleaned protein G-Sepharose (17-0885-02, GE Healthcare) was added and incubated for 1 h at 4°C with rotation. The beads were washed three times with ice-cold extraction buffer, mixed with protein loading buffer, and boiled for 10 min, and the immunoprecipitated proteins were analyzed by western blot.

ChIP-qPCR

ChIP assays were performed as described previously [47]. Briefly, *N. crassa* tissues were fixed with 1% formaldehyde for 15 min at 25°C with shaking and then quenched with glycine at a final concentration of 125 mM for 5 min. Cross-linked tissues were ground and resuspended at 0.5 g/6 ml in lysis buffer containing 1 mM PMSF (Phenylmethylsulfonyl fluoride), 1 μg/ml pepstatin A, and 1 μg/ml leupeptin. Chromatin was

sheared by sonication to ~300 bp fragments. Equal amounts of total protein (2 mg protein/ml) were used per immunoprecipitation, and 10 μl was kept as the input DNA. ChIP was carried out with 2.5 μl of antibody to H3 (BE3015, EASYBIO), 3 μl of antibody to H3ac (06-599, Millipore), 3 μl of antibody to H4ac (06-866, Millipore), 10 μl of antibody to H4 (14149S, CST), 8 μl of antibody to INO80 [48], 10 μl of antibody to NC2α [17], 10 μl of antibody to TFIIB [17], 10 μl of antibody to H2A.Z [16], 10 μl of antibody to VIB-1, or 5 μl of antibody to RPB-1 [49]. Finally, immunoprecipitated DNA was quantified using real-time PCR with primer pairs (see Supplementary Table S1). Recruitments or occupancies data were normalized by the input DNA and presented as a percentage of input DNA.

Results

VIB-1 is a positive regulator of *cat-3* transcription in a dose-dependent manner

To investigate factors regulating catalase expression in *Neurospora crassa*, we screened transcription factor mutants (in the *band* background) and found that the *vib-1*^{KO} mutant is sensitive to H_2O_2. As shown in Fig. 1A and B, the *vib-1*^{KO} strain showed a H_2O_2-sensitive phenotype compared to that of the WT strain. To further confirm the H_2O_2-sensitive phenotype of the *vib-1*^{KO} strain, a construct carrying the sequence encoding the Myc-tagged VIB-1 driven by a strong promoter of the *cfp* gene (NCU02193) was transformed into the *vib-1*^{KO} strain. The ectopic expression of Myc-VIB-1 rescued the H_2O_2-sensitive phenotype of the *vib-1*^{KO} strain to that of the WT strain (Fig. 1A and B), indicating that the observed phenotype was due to the deletion of the *vib-1* gene. Since catalases could be secreted in response to oxidative stress in the environment, we examined the activity of catalases using a stained colonies experiment in the WT, *vib-1*^{KO}, and *vib-1*^{KO};Myc-VIB-1 transformant strains. A large halo representing catalase activity was observed in the WT and *vib-1*^{KO};Myc-VIB-1 colonies, but it was significantly smaller around the *vib-1*^{KO} colonies (Fig. 1C). Then, we examined the zymogram of catalases in the WT, *vib-1*^{KO}, and *vib-1*^{KO};Myc-VIB-1 strains by an in-gel assay. As shown in Fig. 1D, the band corresponding to CAT-3 activity was extremely weak in the *vib-1*^{KO} strain compared to that in the WT and *vib-1*^{KO};Myc-VIB-1 strains. These data indicate that VIB-1 positively regulates the CAT-3 activity.

A previous study showed that the level of *cat-3* mRNA was decreased in the *vib-1* mutant compared with that of the WT strain under conditions with BSA, Xylan, or no carbon medium [35]. Consistently, western blot and RT-qPCR analyses revealed that the levels of CAT-3 protein and *cat-3* mRNA were reduced in the *vib-1*^{KO} strain compared to those in the WT and *vib-1*^{KO};Myc-VIB-1 strains (Fig. 1E and F). To compare the protein levels of Myc-VIB-1 driven by *cfp* promoter in *vib-1*^{KO};Myc-VIB-1 strain and endogenous VIB-1 in WT strains, we generated a VIB-1-specific antibody that recognized a specific band at the predicted molecular weight in the WT strain but not in the *vib-1*^{KO} strain (Supplementary Fig. S1). Western blot analysis revealed that Myc-VIB-1 protein level in *vib-1*^{KO};Myc-VIB-1 strain was higher than the endogenous VIB-1 in the WT strain (Fig. 1E). Taken together, these results confirm that VIB-1 is a positive regulator of *cat-3* transcription in *N. crassa*.

To test whether VIB-1 overexpression in WT can further elevate *cat-3* transcription, we generated the *wt;*Myc-VIB-1 transformants to measure the expression levels of *cat-3*. Western blot analysis revealed that the level of Myc-VIB-1 driven by *cfp* promoter is higher than VIB-1 levels in the WT and *wt*;Myc-VIB-1 strain (Fig. 2A). Consistent with the VIB-1 overexpression, the levels of CAT-3 protein, CAT-3 activity, and *cat-3* mRNA were significantly increased in the *wt*;Myc-VIB-1 strain compared to those of the WT and *vib-1*^{KO} strains (Fig. 2A–C). Plate assays showed that although VIB-1 overexpression reduced the growth rate, the transformant exhibited resistance to H_2O_2 treatment compared to the WT strain (Fig. 2D and E). Taken together, these results indicate that VIB-1 positively regulates *cat-3* expression in a dose-dependent manner.

The DNA-binding activity of VIB-1 contributes to *cat-3* activation

Early studies on Ndt80-like transcription factors began with the sporulation-specific transcription factor Ndt80p in *Saccharomyces cerevisiae*, which identified the DNA-binding domain of Ndt80p and revealed that Ndt80p belongs to the Ig-fold family of transcription factors [50, 51]. Subsequently, introducing amino acid substitutions at DNA-contacting residues indicated that many of these mutations significantly reduced DNA-binding affinity and transcriptional activity [52]. Through amino acid sequence alignment of the *S. cerevisiae* Ndt80p protein with those from other organisms, the DNA-binding domain of Ndt80p was found to be highly conserved in filamentous fungi (Supplementary Fig. S2A) [50, 52, 53]. This domain is located at residues 185–350 of the *N. crassa* VIB-1 protein. Residues K110, R111, and R254, which have been shown to reduce DNA-binding affinity upon mutation in *S. cerevisiae*, correspond to R190, R191, and R291 in *N. crassa* VIB-1 protein (Supplementary Fig. S2A). To test the role of the DNA-binding activity of VIB-1 for *cat-3* expression and H_2O_2 sensitivity, we made the *pcfp*-Myc-VIB-1^{R190AR191A}, *pcfp*-Myc-VIB-1^{R290AR291A}, or *pcfp*-Myc-VIB-1$^{\triangle DBD}$ construct and transformed each of them into the *vib-1*^{KO} strain, respectively. Plate assays showed that ectopic expression of Myc-VIB-1 but not Myc-VIB-1^{R190AR191A}, Myc-VIB-1^{R290AR291A}, or Myc-VIB-1$^{\triangle DBD}$ proteins rescued the H_2O_2-sensitivity of the *vib-1*^{KO} strain to that of the WT strain (Supplementary Fig. S2B and C). RT-qPCR analysis revealed that *myc-vib-1* mRNA levels driven by the *cfp* promoter significantly increased in the *vib-1*^{KO} strains compared to the *vib-1* mRNA levels in the WT strain (Fig. 3A). Similarly, protein levels of Myc-VIB-1 and VIB-1 mutants in the *vib-1*^{KO} strains, but not VIB-1$^{\triangle DBD}$ proteins, were significantly increased compared to those in the WT strain (Fig. 3B), indicating that the deletion of the DBD from the VIB-1 protein may affect its stability. Consistent with the phenotypic results, the low levels of CAT-3 activity, transparent halo, CAT-3 protein, and *cat-3* mRNA in the *vib-1*^{KO} strain were rescued by Myc-VIB-1, but not by the DNA-binding deficient proteins (Fig. 3C–F), indicating that the DNA binding activity of VIB-1 is required for *cat-3* activation.

We then examined the overexpression of VIB-1 protein with a deficient DNA-binding domain in the WT background and found that overexpression of Myc-VIB-1 but not the mutant VIB-1 increased resistance to H_2O_2 treatment compared to that in the WT strain (Supplementary Fig. S3A and B), suggest-

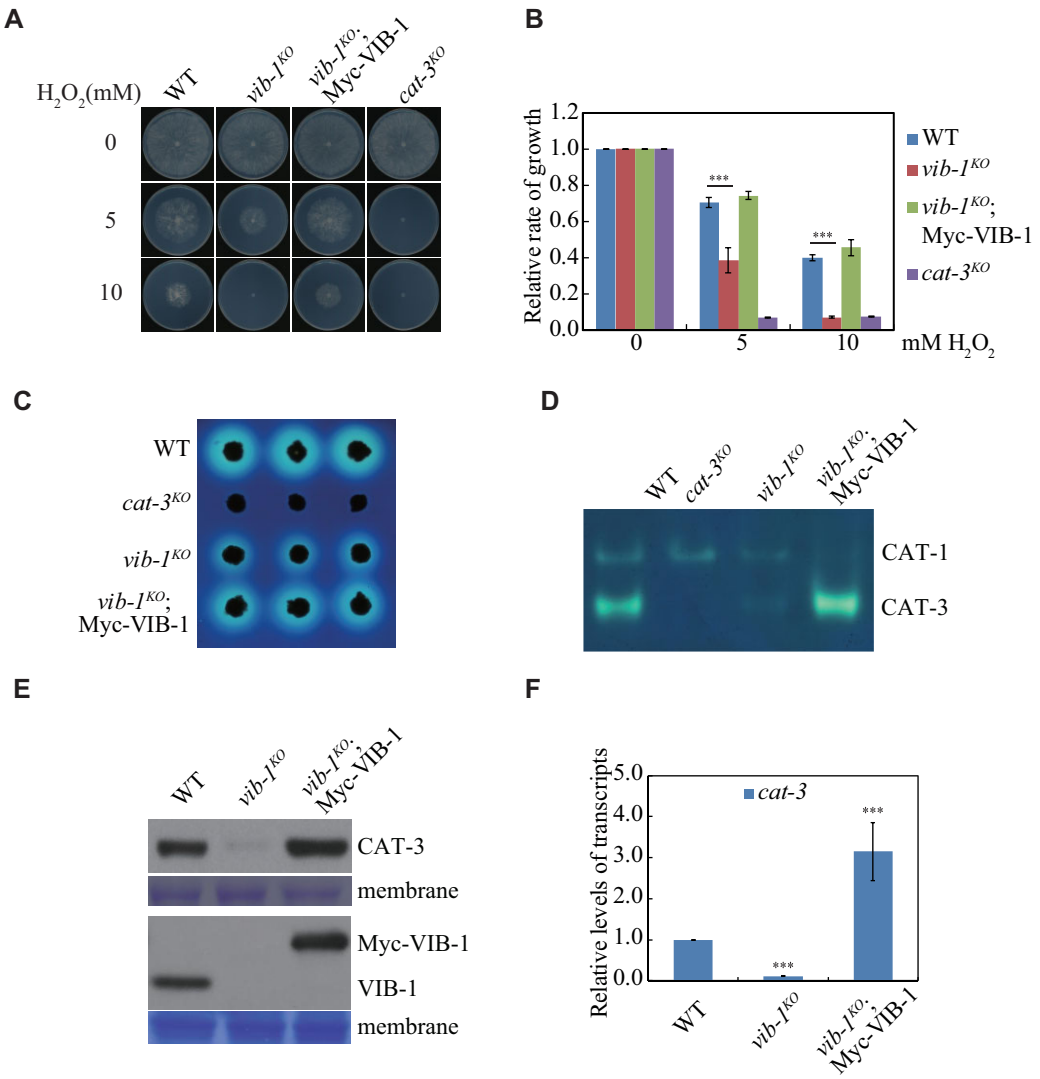

Figure 1. Deletion of VIB-1 causes a H_2O_2-sensitive phenotype and low levels of CAT-3 expression. (**A**) Plate assays analyzing mycelial growth of WT, *vib-1*^{KO}, *vib-1*^{KO};Myc-VIB-1 and *cat-3*^{KO} strains under 0, 5, or 10 mM H_2O_2 concentrations. Cultures were inoculated in plates at 25°C under constant light. (**B**) Quantitation of growth relative to WT, *vib-1*^{KO}, *vib-1*^{KO};Myc-VIB-1, and *cat-3*^{KO} strains under conditions described in panel (A). (**C**) Extracellular catalases assay showing the levels of extracellular catalases activity in the WT, *cat-3*^{KO}, *vib-1*^{KO}, and *vib-1*^{KO};Myc-VIB-1 strains. (**D**) In-gel assay analysis of the CAT-3 activity levels in WT, *cat-3*^{KO}, *vib-1*^{KO}, and *vib-1*^{KO};Myc-VIB-1 strains. (**E**) Western blot analyses showing the levels of CAT-3 and VIB-1 protein in the WT, *vib-1*^{KO}, and *vib-1*^{KO};Myc-VIB-1 strains. The membranes stained by Coomassie Blue represent the total protein in each sample and act as a loading control for the western blot. (**F**) RT-qPCR assays analyzing the levels of *cat-3* mRNA in the WT, *vib-1*^{KO}, and *vib-1*^{KO};Myc-VIB-1 strains. Error bars indicate SD ($n = 3$). Significance was evaluated by two-tailed *t*-test; $***P < 0.001$.

ing that overexpression of Myc-VIB-1 with the DNA-binding defect mutation in the WT background has no effect on endogenous VIB-1 function. Consistent with the phenotypic results, CAT-3 activity and CAT-3 protein levels were increased by overexpression of Myc-VIB-1, but not by its DNA-binding domain mutants (Supplementary Fig. S3C and D).

To confirm whether VIB-1 activates *cat-3* transcription by directly binding to its promoter, we performed ChIP assays with VIB-1-specific antibodies in WT, *vib-1*^{KO}, and transformant strains. ChIP assays showed that VIB-1 could be enriched in the promoter and TSS of the *cat-3* gene in the WT and *vib-1*^{KO};Myc-VIB-1 strains (Fig. 3G and H), whereas the enrichments were abolished in *vib-1*^{KO};Myc-VIB-1^{R190AR191A}, *vib-1*^{KO};Myc-VIB-1^{R290AR291A}, and *vib-1*^{KO};Myc-VIB-1$^{\Delta DBD}$ strains (Fig. 3H). Consistent with the elevated expression of *cat-3*, the enrichment of VIB-1 was dramatically increased in the *wt*;Myc-VIB-1 transformant compared to that in the WT strain (Fig. 3I). These results demonstrate that the DNA-binding activity of VIB-1 is required for *cat-3* activation.

VIB-1 activates its target genes by decreasing the nucleosome density at these loci

To determine whether the binding of VIB-1 facilitates the recruitment of transcription PIC at the *cat-3* locus, we measured the recruitment of TFIIB and RPB-1 in the WT, *vib-1*^{KO}, and *wt*;Myc-VIB-1 strains by ChIP assays using TFIIB- or RPB-1-specific antibodies. The recruitment levels of TFIIB and RPB-1 at the *cat-3* TSS and ORF regions decreased in the *vib-1*^{KO} strain and increased significantly in the *wt*;Myc-VIB-1 strain compared with WT strain (Fig. 4A and B). These results indicate that VIB-1 activates *cat-3* transcription by recruiting or stabilizing the transcription PIC.

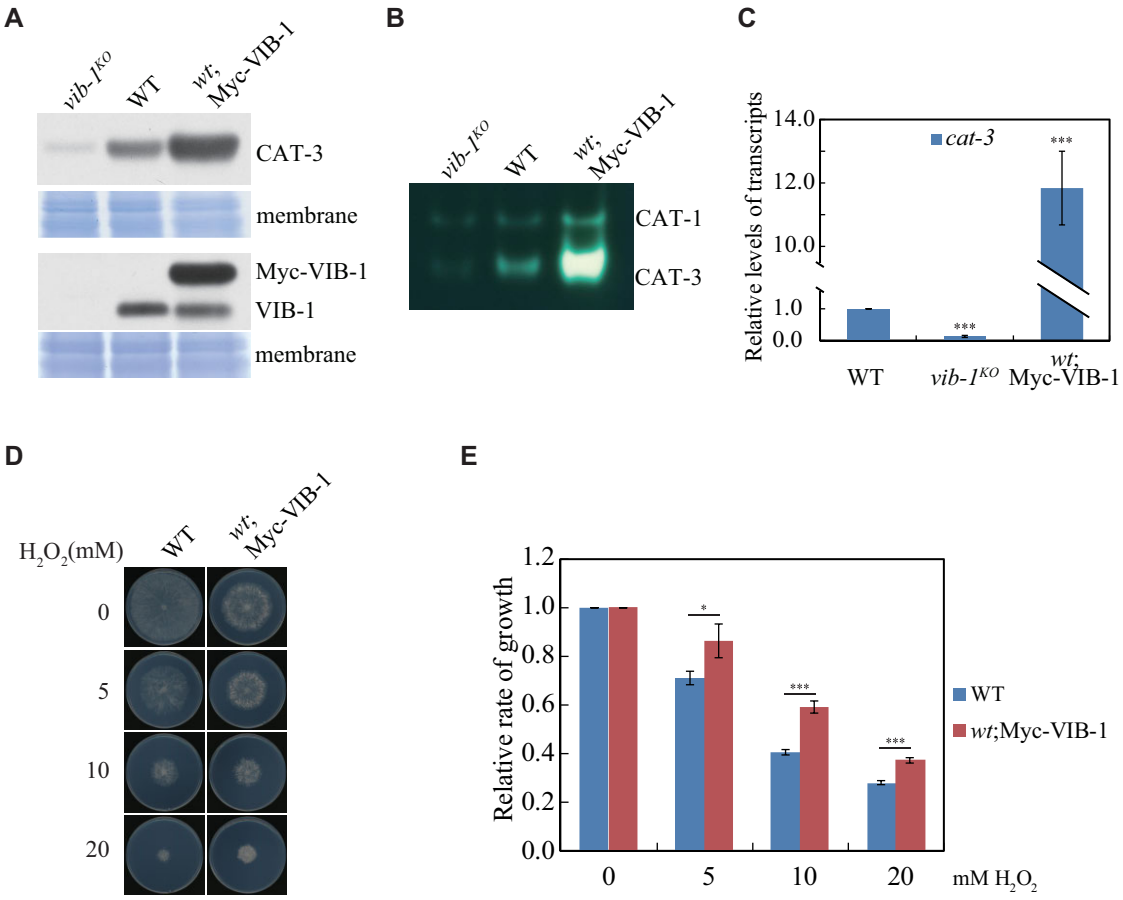

Figure 2. VIB-1 overexpression strains exhibit increased CAT-3 expression and are resistant to H_2O_2. (**A**) Western blot analyses showing the levels of CAT-3 and VIB-1 protein in the WT, *vib-1*^{KO}, and *wt*;Myc-VIB-1 strains. The membranes stained by Coomassie Blue represent the total protein in each sample and act as a loading control for the western blot. (**B**) In-gel assay analysis of the CAT-3 activity levels in WT, *vib-1*^{KO}, and *wt*;Myc-VIB-1 strains. (**C**) RT-qPCR assays analyzing the levels of *cat-3* mRNA in the WT, *vib-1*^{KO}, and *wt*;Myc-VIB-1 strains. (**D**) Plate assay analysis showing mycelial growth of WT and *wt*;Myc-VIB-1 strains on plates with 0, 5, 10, or 20 mM H_2O_2 as indicated. Cultures were inoculated in plates at 25°C under constant light. (**E**) Quantitation of growth relative to WT and *wt*;Myc-VIB-1 strains under conditions described in panel (D). Error bars indicate SD ($n = 3$). Significance was evaluated by two-tailed *t*-test; $*P < 0.05$, $***P < 0.001$.

We previously found that a transcriptional activator, CPC1/GCN4, binds to the *cat-3* promoter and coordinates with the histone acetyltransferase NGF-1/GCN5 to acetylate histone H3 at the nucleosomes of the *cat-3* promoter and TSS [15]. ChIP assays showed that the levels of H3 and H4 at the *cat-3* promoter and TSS in the *vib-1*^{KO} strain were higher than those in the WT strain (Fig. 4C and D). However, overexpression of VIB-1 in the WT strain reduced the nucleosome density at the *cat-3* promoter and TSS compared to those in the WT strain (Fig. 4C and D), indicating that VIB-1 functions to reduce nucleosome density at the promoter and TSS of the *cat-3* gene. ChIP data revealed that overexpression of VIB-1 in the WT strain significantly increased the H3ac levels but not the H4ac levels at the *cat-3* promoter and TSS compared to those in the WT and *vib-1*^{KO} strains (Fig. 4E and F), indicating that VIB-1 activates *cat-3* expression by decreasing the nucleosome density at the *cat-3* gene.

In a study on *N. crassa* regarding the regulatory and transcriptional mechanisms governing carbon utilization, 238 direct target genes of VIB-1 were identified through DNA affinity purification sequencing (DAP-seq) and RNA-seq analysis [35]. To determine whether the mechanism of VIB-1 is conserved in other target genes, we selected two VIB-1 target genes, NCU05841 and NCU02904, for validation. Results from the VIB-1 ChIP assay indicated that VIB-1 is recruited to these target genes (Supplementary Fig. S4A). Compared to the WT strain, the expression levels of NCU05841 and NCU02904 genes were reduced in the *vib-1*^{KO} strain, while their expression levels were increased in the *wt*;Myc-VIB-1 strain (Supplementary Fig. S4B). These results further confirmed that these genes are indeed VIB-1 target genes. Similar to the case of the *cat-3* gene locus, the recruitment levels of TFIIB and RPB-1 at the TSS or downstream regions of the NCU05841 and NCU02904 genes decreased in the *vib-1*^{KO} strain and increased in the *wt*;Myc-VIB-1 strain compared with WT strain (Supplementary Fig. S5A and B). Consistent with the *cat-3* gene, the levels of H3 at the TSS of these VIB-1 target genes were elevated in the *vib-1*^{KO} strain but reduced in the VIB-1 overexpression strain compared to those in the WT strain (Supplementary Fig. S5C). ChIP assays also showed that overexpression of VIB-1 in the WT strain significantly increased the H3ac levels at the TSS of the NCU05841 and NCU02904 genes compared to those in the WT and *vib-1*^{KO} strains (Supplementary Fig. S5D). Taken together, these results indicate that VIB-1 activates target gene transcription by recruiting or stabilizing the transcription PIC and

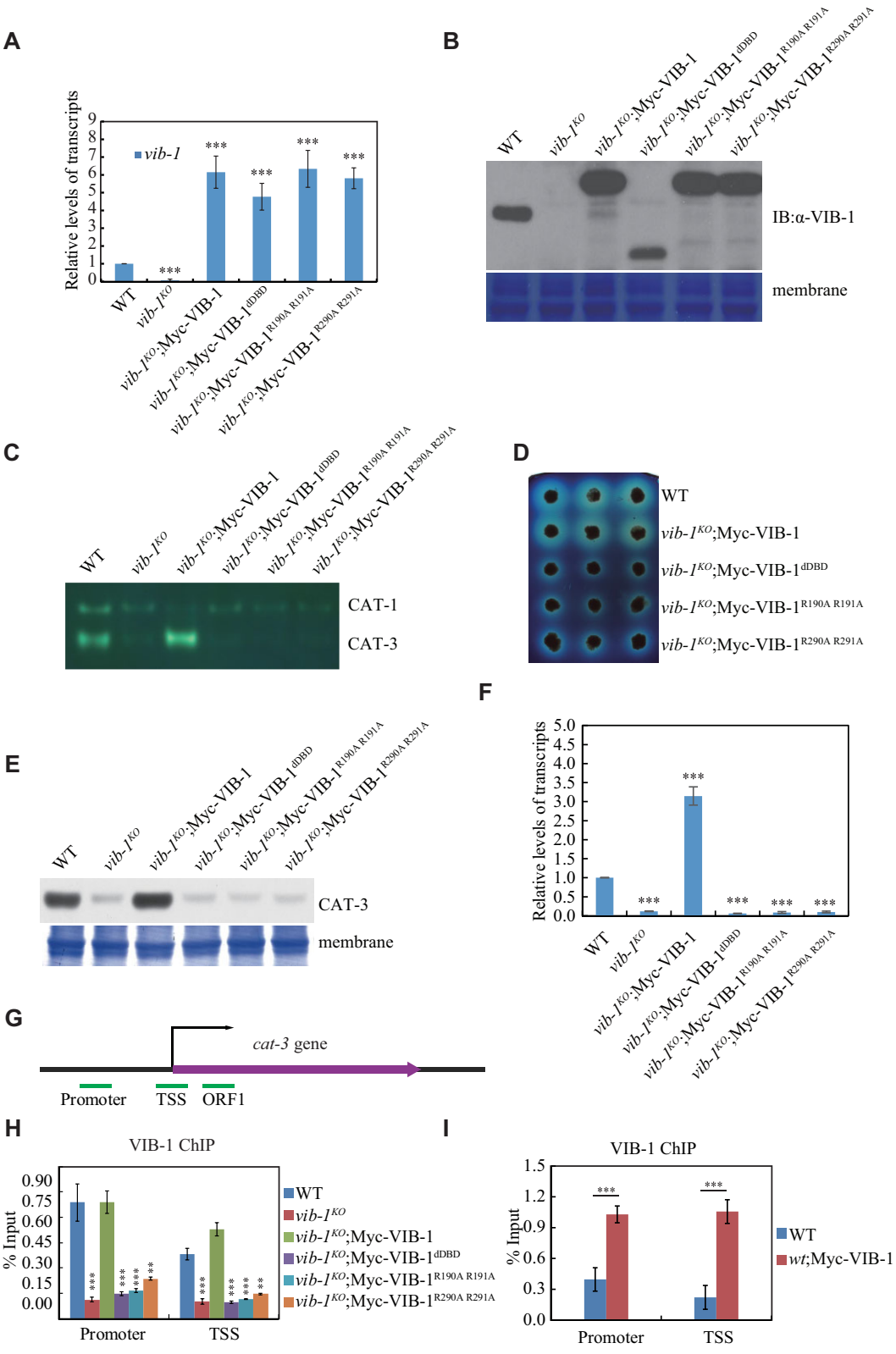

Figure 3. VIB-1 activates the transcription of *cat-3* via its DNA-binding activity. (**A**) RT-qPCR assays analyzing the levels of *vib-1* mRNA in the WT, *vib-1*^{KO}, and VIB-1 transformants. (**B**) Western blot analyses showing the levels of VIB-1 protein in the WT, *vib-1*^{KO}, and VIB-1 transformants. The membranes stained by Coomassie Blue represent the total protein in each sample and act as a loading control for the western blot. (**C**) In-gel assay analysis of the CAT-3 activity levels in WT, *vib-1*^{KO}, and VIB-1 transformants. (**D**) Extracellular catalases assay showing the levels of extracellular catalases activity in the WT, *vib-1*^{KO}, and VIB-1 transformants. (**E**) Western blot analyses showing the levels of CAT-3 protein in the WT, *vib-1*^{KO}, and VIB-1 transformants. The membranes stained by Coomassie Blue represent the total protein in each sample and act as a loading control for the western blot. (**F**) RT-qPCR assays analyzing the levels of *cat-3* mRNA in the WT, *vib-1*^{KO}, and VIB-1 transformants. (**G**) Schematic depicting the *cat-3* gene. Promoter, TSS and ORF1 indicate the regions tested by ChIP-qPCR; ORF, open reading frame. ORF1 refers to the ChIP-qPCR primer pair located in the first ORF region of the *cat-3* gene, 330 bp downstream of the TSS. (**H** and **I**) ChIP assays showing the binding levels of VIB-1 at Promoter/TSS regions of *cat-3* gene in WT, *vib-1*^{KO}, and VIB-1 transformants. Error bars indicate SD ($n = 3$). Significance was evaluated by two-tailed *t*-test; $^{**}P < 0.01$, $^{***}P < 0.001$.

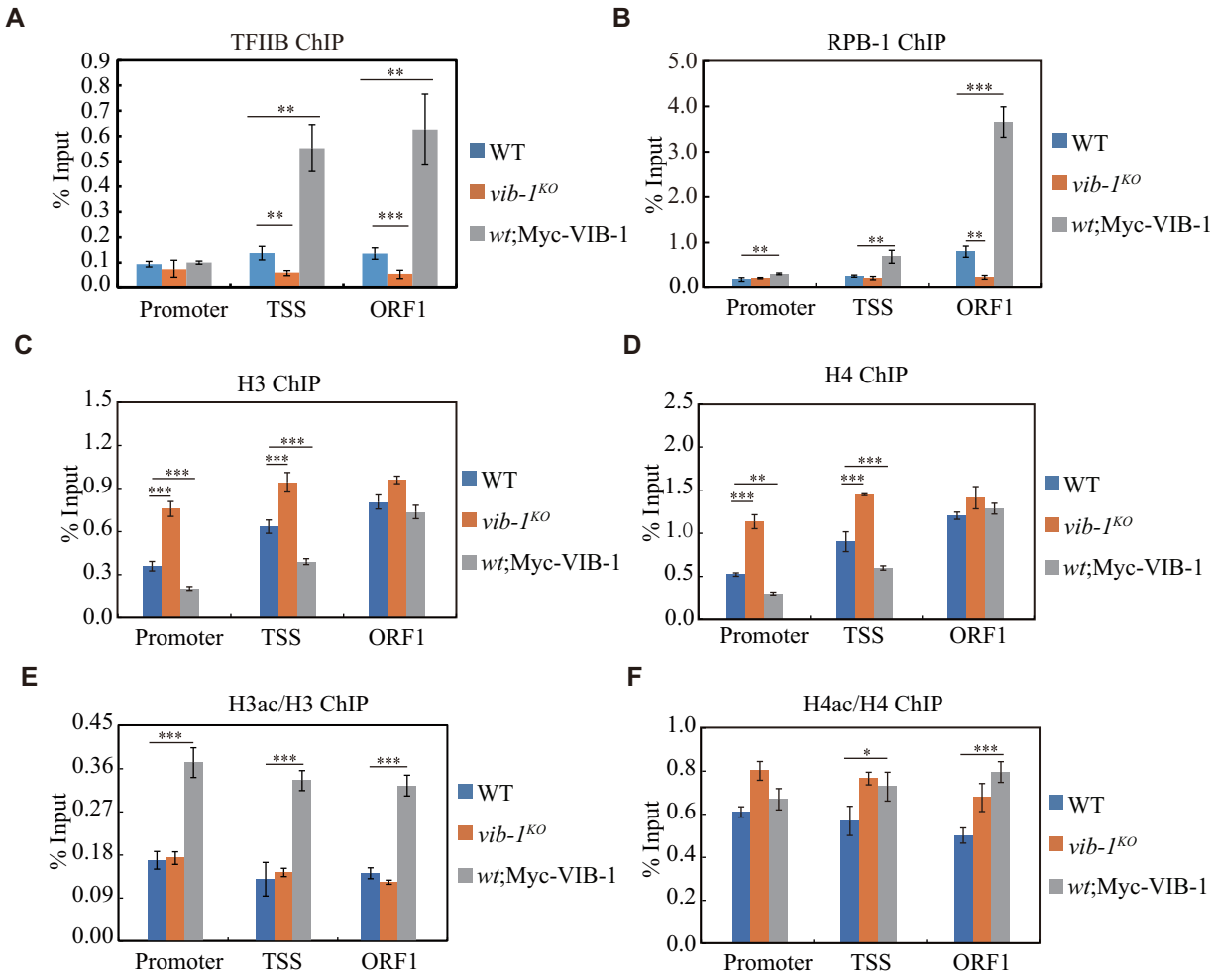

Figure 4. VIB-1 activates *cat-3* expression by decreasing the nucleosome density at the *cat-3* gene. (**A** and **B**) ChIP analyses showing the recruitment of TFIIB (A) and RPB-1 (B) at different regions of the *cat-3* gene in WT, *vib-1*^{KO}, and *wt*;Myc-VIB-1 strains. (**C** and **D**) ChIP assays showing the occupancy levels of histone protein H3 (C) and histone protein H4 (D) at the *cat-3* locus in WT, *vib-1*^{KO}, and *wt*;Myc-VIB-1 strains. (**E** and **F**) ChIP analyses showing the enrichment of H3ac (E) and H4ac (F) and at different regions of the *cat-3* gene in WT, *vib-1*^{KO}, and *wt*;Myc-VIB-1 strains. The locations detected by the ChIP assay are indicated in (Fig. 3G). Error bars indicate SD ($n = 3$). Significance was evaluated by two-tailed *t*-test; $^{**}P < 0.01$, $^{***}P < 0.001$.

decreasing nucleosome density at the recruitment sites, demonstrating a general mechanism.

VIB-1 overexpression bypasses CPC1 activity for *cat-3* activation

To evaluate the relationship between VIB-1 and CPC-1 for *cat-3* activation, we first examined the levels of VIB-1 protein in WT and *cpc-1* (j-5) strains. The *cpc-1 (j-5)* strain is a mutant of *N. crassa* generated previously [54], in which a translocation occurred in the promoter region of the *cpc-1* gene, preventing transcription of *cpc-1* mRNA and thereby abolishing the expression of the CPC-1 protein. Western blot analysis revealed reduced levels of VIB-1 protein in the *cpc-1* mutant compared to those in the WT strain (Fig. 5A). To test whether the low expression of *cat-3* in the *cpc-1* mutant can be rescued by overexpression of VIB-1, we introduced the *pcfp*-Myc-VIB-1 plasmid into the *cpc-1* (j-5) mutant. Plate assays showed that overexpression of VIB-1 partially restored the H_2O_2-sensitive phenotype of the *cpc-1* (j-5) mutant (Fig. 5B and C). Consistent with the phenotypic results, the low levels of *cat-3* mRNA, CAT-3 protein, and CAT-3 activity in the *cpc-1* (j-5) mutant were rescued to the WT levels by VIB-1 overexpression (Fig. 5D–F). Recently, we found that mutants of the UPF complex factors exhibit strong H_2O_2-resistant phenotypes and elevated *cat-3* expression via increased CPC-1 protein [42]. To further determine the genetic interaction between *vib-1* and *upf* in the *cat-3* activation process, we generated the *upf3*^{KO};*vib-1*^{KO} double mutant and examined the H_2O_2 sensitivity of the double mutant. Similar to the *vib-1* single mutant, this double mutant also exhibited H_2O_2-sensitive phenotypes (Fig. 5G and H), indicating that the loss of VIB-1 reversed the H_2O_2-resistant phenotype of the *upf* mutant. Consistent with these phenotypes, elevated levels of CAT-3 activity and CAT-3 protein in the *upf-3*^{KO} strain were significantly decreased in the absence of VIB-1 (Fig. 5I and J), further demonstrating that VIB-1 activates *cat-3* downstream of CPC-1 activity.

VIB-1 overexpression also bypasses NC2α activity for *cat-3* activation

In *N. crassa*, the histone variant H2A.Z is incorporated into nucleosomes at the *cat-3* locus through a chromatin remodeling complex, the SWR1 complex, and acts as a negative regulator of *cat-3* gene expression [55]. Negative cofactor 2 (NC2) is a conserved histone-fold transcriptional

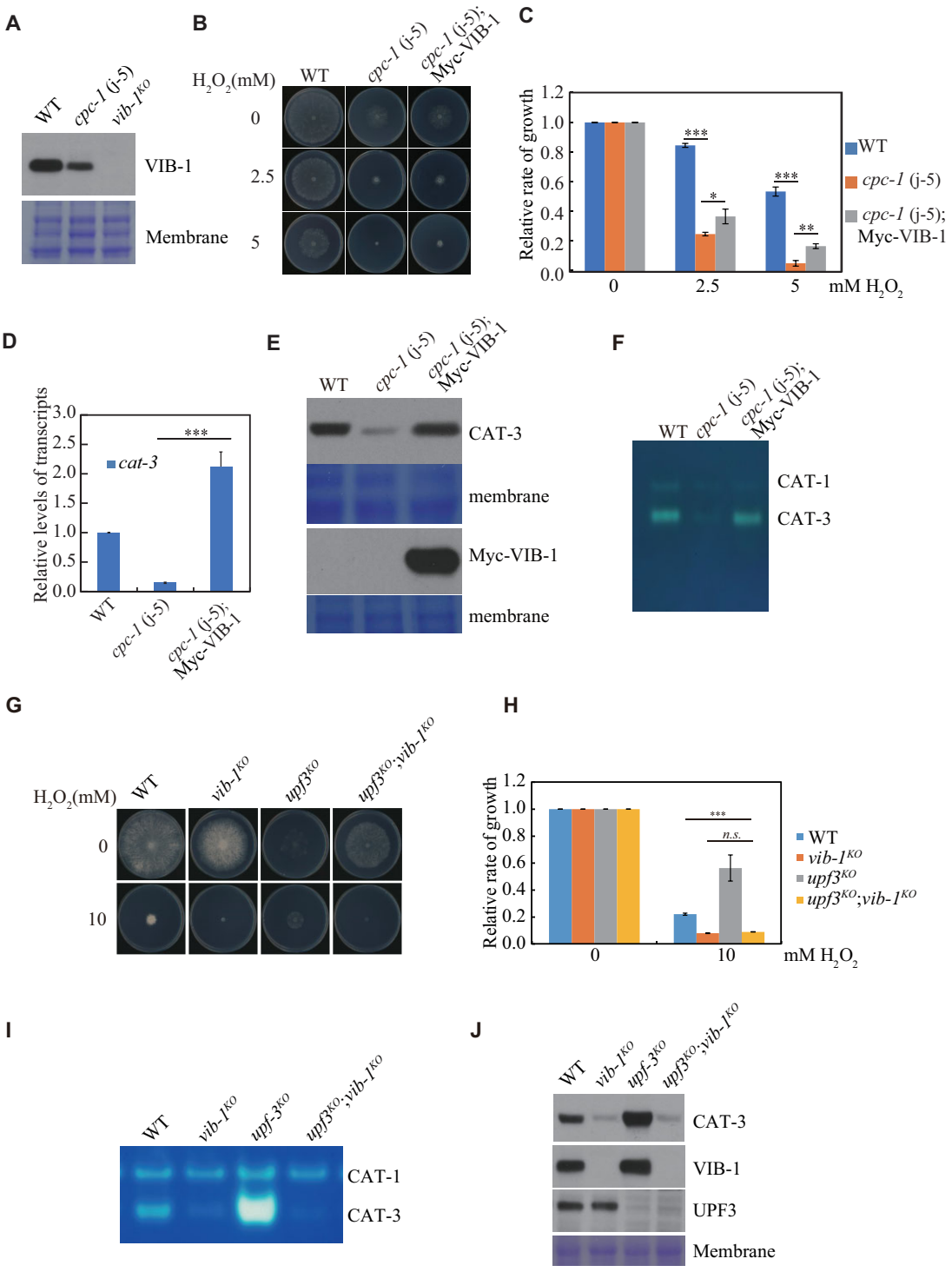

Figure 5. VIB-1 overexpression bypasses CPC1 activity for *cat-3* activation. (**A**) Western blot analyses showing the levels of VIB-1 protein in the WT, *cpc-1* (j-5), *vib-1*^{KO} strains. The membranes stained by Coomassie Blue represent the total protein in each sample and act as a loading control for the western blot. (**B**) Plate assay analysis showing mycelial growth of WT, *cpc-1* (j-5), and *cpc-1* (j-5);Myc-VIB-1 strains on plates with 0, 2.5, or 5 mM H_2O_2 as indicated. Cultures were inoculated in plates at 25°C under constant light. (**C**) Quantitation of growth relative to WT, *cpc-1* (j-5), and *cpc-1* (j-5);Myc-VIB-1 strains under conditions described in panel (B). (**D**) RT-qPCR assays analyzing the levels of *cat-3* mRNA in WT, *cpc-1* (j-5), and *cpc-1* (j-5);Myc-VIB-1 strains. (**E**) Western blot analyses showing the levels of CAT-3 and VIB-1 protein in the WT, *cpc-1* (j-5), and *cpc-1* (j-5);Myc-VIB-1 strains. The membranes stained by Coomassie Blue represent the total protein in each sample and act as a loading control for the western blot. (**F**) In-gel assay analysis of the CAT-3 activity levels in WT, *cpc-1* (j-5), and *cpc-1* (j-5);Myc-VIB-1 strains. (**G**) Plate assay analysis showing mycelial growth of WT, *vib-1*^{KO}, *upf3*^{KO}, and *upf3*^{KO};*vib-1*^{KO} strains on plates with 0 or 10 mM H_2O_2 as indicated. Cultures were inoculated in plates at 25°C under constant light. (**H**) Quantitation of growth relative to WT, *vib-1*^{KO}, *upf3*^{KO}, and *upf3*^{KO};*vib-1*^{KO} strains under conditions described in panel (G). (**I**) In-gel assay analysis of the CAT-3 activity levels in WT, *vib-1*^{KO}, *upf3*^{KO}, and *upf3*^{KO};*vib-1*^{KO} strains. (**J**) Western blot analyses showing the levels of CAT-3, VIB-1, and UPF3 protein in the WT, *vib-1*^{KO}, *upf3*^{KO}, and *upf3*^{KO};*vib-1*^{KO} strains. The membranes stained by Coomassie Blue represent the total protein in each sample and act as a loading control for the western blot. Error bars indicate SD ($n = 3$). Significance was evaluated by two-tailed *t*-test; n.s., $P > 0.05$, $^{*}P < 0.05$, $^{**}P < 0.01$, $^{***}P < 0.001$.

regulator in eukaryotes [56–60]. Our previous data showed that NC2α/β positively regulates *cat-3* transcription through recruiting the chromatin remodeling INO80 complex, which removes H2A.Z from the *cat-3* promoter/TSS regions [17]. Thus, we examined the occupancies of H2A.Z, NC2α, and INO80 at the *cat-3* promoter and TSS in the WT, *vib-1*^{KO}, and *wt*;Myc-VIB-1 strains. ChIP assays showed that the loss of VIB-1 dramatically increased the occupancy of H2A.Z and decreased the enrichment of NC2α and INO80 at the *cat-3* promoter and TSS compared to those of the WT and *wt*;Myc-VIB-1 strains (Fig. 6A and B, and Supplementary Fig. S6), suggesting that VIB-1 activates *cat-3* expression by antagonizing the inhibition of H2A.Z around the *cat-3* promoter and TSS. To test this possibility, we generated the *vib-1*^{KO};*H2A.Z*^{KO} double mutant, and found that deletion of H2A.Z reversed the sensitive phenotype of the *vib-1*^{KO} strain in response to H_2O_2-induced oxidative stress (Fig. 6C and D). Consistently, in-gel assays and western blot analyses showed that the low levels of CAT-3 activity and CAT-3 protein in the *vib-1*^{KO} strain were reversed by the deletion of H2A.Z compared to those in the WT strain, and these levels were still lower than those in the *H2A.Z*^{KO} or *wt*;Myc-VIB-1 strains (Fig. 6E and F). Unexpectedly, the mRNA levels of *cat-3* in the *vib-1*^{KO};*H2A.Z*^{KO} double mutant were significantly lower than those in the *H2A.Z*^{KO} and *wt*;Myc-VIB-1 strains (Fig. 6G), indicating that VIB-1 plays a crucial role in *cat-3* activation. The ChIP assay further showed that the recruitment of TFIIB and RPB-1 at the *cat-3* TSS and ORF region in the *wt*;Myc-VIB-1 strain was significantly increased, while the recruitment of TFIIB and RPB-1 in the *H2A.Z*^{KO} and *vib-1*^{KO};*H2A.Z*^{KO} strains was comparable with the WT strain (Fig. 6H and I). Taken together, these results suggest that VIB-1 activates *cat-3* transcription through recruiting TFIIB and RNA polymerase II (RNAPII), which results in decreased H2A.Z from the *cat-3* promoter and TSS.

To test whether VIB-1 overexpression also bypasses NC2 activity for *cat-3* activation, we generated the *Nc2α*^{KO};Myc-VIB-1 transformants by introducing the *pcfp*-Myc-VIB-1 plasmid into the *Nc2α*^{KO} strain. As expected, plate assays showed that the H_2O_2-sensitive phenotype of the *Nc2α*^{KO} strain was partially restored by VIB-1 overexpression compared to those of the WT and *Nc2α*^{KO} strains (Fig. 7A and B). Consistently, VIB-1 overexpression restored the low levels of *cat-3* mRNA, CAT-3 protein, and CAT-3 activity in the *Nc2α*^{KO} strain to WT levels (Fig. 7C–E). ChIP assays showed that VIB-1 binding levels at the *cat-3* promoter and TSS were significantly decreased in the *Nc2α*^{KO} strain, whereas VIB-1 overexpression restored VIB-1 binding levels in the *Nc2α*^{KO} mutant to WT levels (Fig. 7F). Similarly, VIB-1 overexpression reduced the levels of H2A.Z deposition at the *cat-3* locus in the *Nc2α*^{KO} strain to those of the WT strain (Fig. 7G). Taken together, these results indicate that VIB-1 overexpression also bypasses the NC2α activity for *cat-3* activation by promoting the assembly of PIC, which results in decreased H2A.Z from the *cat-3* promoter and TSS.

VIB-1 weakly interacts with TFIIB and mediator subunits for facilitating PIC assembly

The low expression of the *cat-3* gene in the *cpc-1* (j-5) and *Nc2α* mutants rescued by VIB-1 overexpression strongly suggests that VIB-1 may facilitate to recruit the transcriptional machinery to the *cat-3* locus. Amino acid sequence alignment showed that the putative activation domain of the *N. crassa* VIB-1 protein had a weak homology with the transcription activator of the herpes virus, ICP4 (Supplementary Fig. S7). Herpes Simplex Virus 1 ICP4 can cooperate with TBP and TFIIB at promoters containing the ICP4-binding site to form a stable, tripartite complex [61–63]. To test the interactions between VIB-1 and *N. crassa* GTFs, we overexpressed Myc-tagged TFIIB, TAF-5, or 11 MED subunits in the WT strain, respectively. Immunoprecipitation assays revealed that overexpressed Myc-TFIIB, MED-17, or MED-21 proteins weakly interacted with endogenous VIB-1, respectively (Supplementary Fig. S8), indicating that VIB-1 interacts with *N. crassa* GTFs for facilitating the recruitment of the transcription machinery at the *cat-3* gene for its activation. To further confirm this possibility, we measured CAT-3 activity in these overexpressed strains. Like the *wt*;*pcfp*-Myc-VIB-1 strain, overexpression of Myc-tagged MED-14, MED-16, or MED-17 in the WT strain increased CAT-3 activity compared to those in the WT strain (Fig. 8A and B). To test whether VIB-1 is essential for activating *cat-3* by the overexpression of MED subunits, we generated the *vib-1*^{KO};*pcfp*-Myc-MED-16 or MED-17 transformants. In-gel assay revealed that the overexpression of these subunits cannot elevate the expression of *cat-3* in the *vib-1*^{KO} background compared with those in WT overexpression strains (Fig. 8C), indicating that VIB-1 is necessary for recruiting the transcription machinery. Taken together, these results indicate that VIB-1 facilitates recruiting and stabilizing the PIC on the *cat-3* promoter for its activation.

To further test the role of putative transcription activation domain of VIB-1 for *cat-3* expression, we constructed pcfp-HA-VIB-1$^{\Delta AD1}$, pcfp-HA-VIB-1$^{\Delta AD2}$, pcfp-HA-VIB-1$^{\Delta AD3}$, and pcfp-HA-VIB-1$^{\Delta AD}$ (complete deletion) constructs and transformed each of them into the *vib-1*^{KO} strain, respectively (Supplementary Fig. S9A). Plate assays showed that ectopic expression of HA-VIB-1^{WT}, as well as the deletion variants, rescued the H_2O_2-sensitivity of the *vib-1* knockout strain to levels comparable to the WT strain (Supplementary Fig. S9B and C). Consistent with these phenotypic observations, the low levels of CAT-3 protein and CAT-3 activity in the *vib-1*^{KO} strain were restored by the expression of the defective HA-VIB-1 proteins (Supplementary Fig. S9D and E). These findings indicate that the putative transcription activation domain of VIB-1 is not required for the activation of *cat-3*. Although TrVIB1 (VIB-1 ortholog from *T. reesei*) and *N. crassa* VIB-1 share 74.1% amino acid identity in their NDT80 DNA-binding domain, they only share 39.5% amino acid identity in their putative transcription activation domain. Consistent with our observation, constitutive expression of *T. reesei vib-1* in an *N. crassa vib-1* mutant can restore growth and cellulolytic enzyme activity [34]. These results strongly suggest that VIB-1 binding to the promoter region mediated by DNA-binding domain is critical for activating expression of its target genes

Discussion

Catalases play important roles in maintaining intracellular ROS homeostasis. In this study, we found that VIB-1 regulates *cat-3* expression to respond to oxidative stress in *N. crassa*. As a Zn2Cys6 transcription factor, VIB-1 directly binds to the *cat-3* promoter region, recruiting the PIC, including TFIIB and RNAPII, to reduce nucleosome density and promote

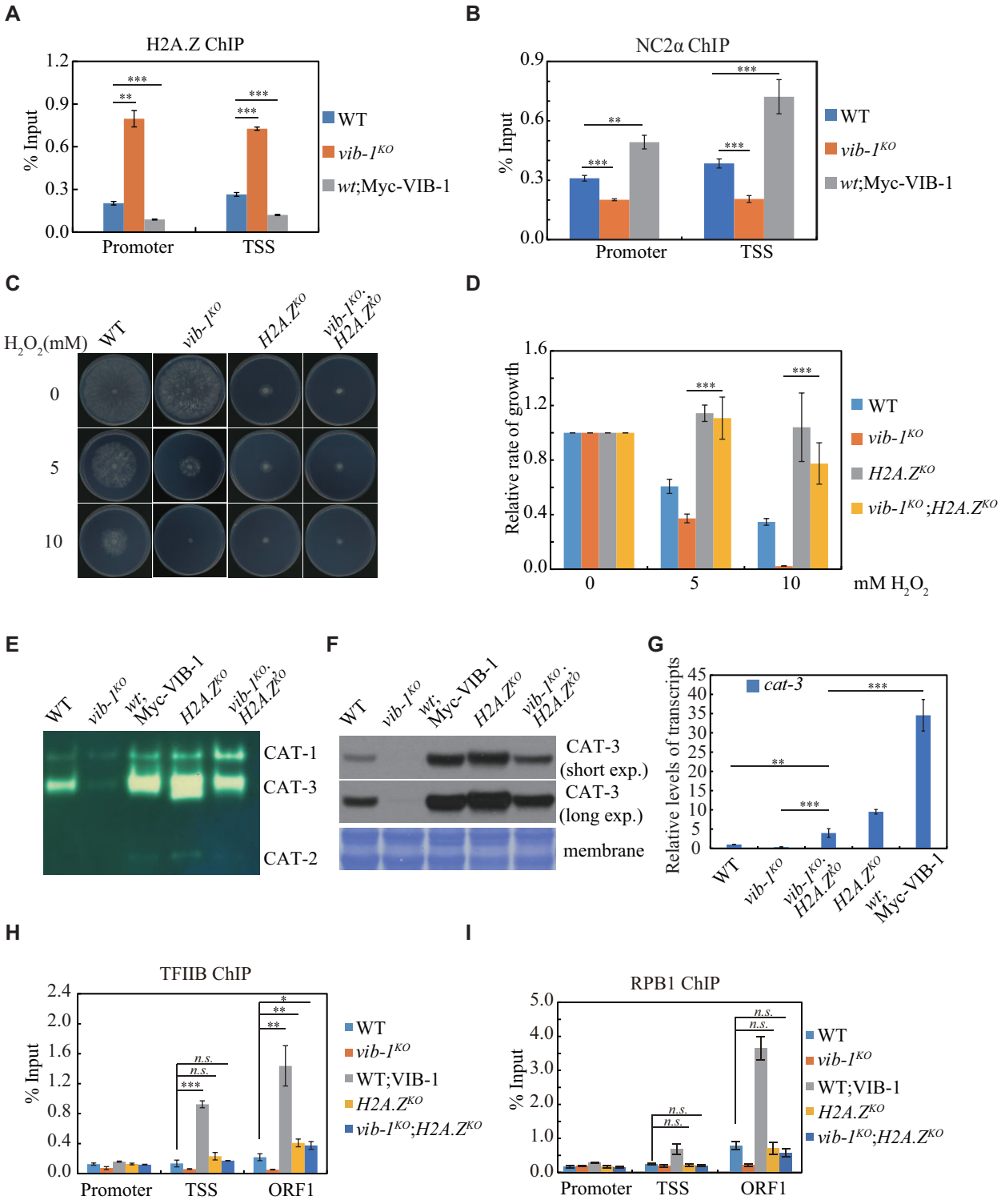

Figure 6. VIB-1 activates *cat-3* transcription by recruiting TFIIB and RNAPII and reducing H2A.Z from the *cat-3* promoter/TSS regions. (**A** and **B**) ChIP assays showing the occupancy levels of H2A.Z (A) and the recruitment of NC2α (B) at the Promoter/TSS regions of the *cat-3* gene in WT, *vib-1*^{KO}, and *wt*;Myc-VIB-1 strains. (**C**) Plate assay analysis showing mycelial growth of WT, *vib-1*^{KO}, *vib-1*^{KO};*H2A.Z*^{KO}, and *H2A.Z*^{KO} strains on plates with 0, 5, or 10 mM H_2O_2 as indicated. Cultures were inoculated in plates at 25°C under constant light. (**D**) Quantitation of growth relative to WT, *vib-1*^{KO}, *vib-1*^{KO};*H2A.Z*^{KO}, and *H2A.Z*^{KO} strains under conditions described in panel (C). (**E**) In-gel assay analysis of the CAT-3 activity levels in WT, *vib-1*^{KO}, *vib-1*^{KO};*H2A.Z*^{KO}, *H2A.Z*^{KO}, and *wt*;Myc-VIB-1 strains. (**F**) Western blot analyses showing the levels of CAT-3 protein in WT, *vib-1*^{KO}, *vib-1*^{KO};*H2A.Z*^{KO}, *H2A.Z*^{KO}, and *wt*;Myc-VIB-1 strains. The membranes stained by Coomassie Blue represent the total protein in each sample and act as a loading control for the western blot. (**G**) RT-qPCR assays analyzing the levels of *cat-3* mRNA in WT, *vib-1*^{KO}, *vib-1*^{KO};*H2A.Z*^{KO}, *H2A.Z*^{KO}, and *wt*;Myc-VIB-1 strains. (**H** and **I**) ChIP analyses showing recruitment of TFIIB (H) and RPB-1 (I) at different regions of the *cat-3* gene in WT, *vib-1*^{KO}, *vib-1*^{KO};*H2A.Z*^{KO}, *H2A.Z*^{KO}, and *wt*;Myc-VIB-1 strains. The locations detected by the ChIP assay are indicated in Fig. 3G. Error bars indicate SD ($n = 3$). Significance was evaluated by two-tailed *t*-test; n.s., $P > 0.05$, $^{*}P < 0.05$, $^{**}P < 0.01$, $^{***}P < 0.001$.

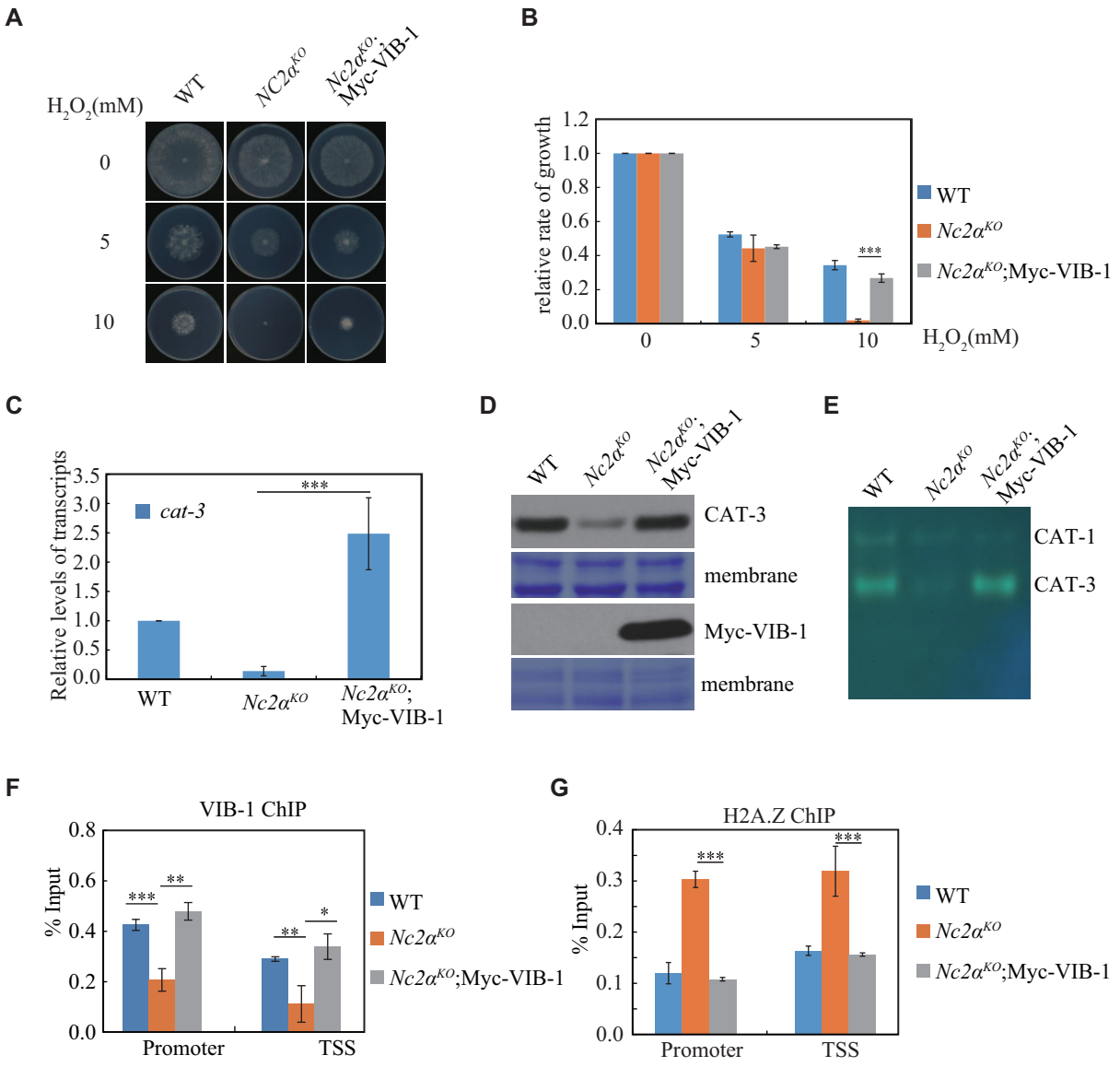

Figure 7. VIB-1 can activate *cat-3* transcription by removing H2A.Z from the *cat-3* locus, bypassing NC2 complex activity. (**A**) Plate assay analysis showing mycelial growth of WT, *Nc2α*^{KO}, and *Nc2α*^{KO};Myc-VIB-1 strains on plates with 0, 5, or 10 mM H_2O_2 as indicated. Cultures were inoculated in plates at 25°C under constant light. (**B**) Quantitation of growth relative to WT, *Nc2α*^{KO}, and *Nc2α*^{KO};Myc-VIB-1 strains under conditions described in panel (A). (**C**) RT-qPCR assays analyzing the levels of *cat-3* mRNA in WT, *Nc2α*^{KO}, and *Nc2α*^{KO};Myc-VIB-1 strains. (**D**) Western blot analyses showing the levels of CAT-3 and VIB-1 protein in the WT, *Nc2α*^{KO}, and *Nc2α*^{KO};Myc-VIB-1 strains. The membranes stained by Coomassie Blue represent the total protein in each sample and act as a loading control for the western blot. (**E**) In-gel assay analysis of the CAT-3 activity levels in WT, *Nc2α*^{KO}, and *Nc2α*^{KO};Myc-VIB-1 strains. (**F** and **G**) ChIP assays showing the recruitment of VIB-1 (F) and the occupancy levels of H2A.Z (G) at the Promoter/TSS regions of the *cat-3* gene in WT, *Nc2α*^{KO}, and *Nc2α*^{KO};Myc-VIB-1 strains. Error bars indicate SD ($n = 3$). Significance was evaluated by two-tailed *t*-test; $*P < 0.05$, $**P < 0.01$, $***P < 0.001$.

cat-3 transcription. Additionally, VIB-1 facilitates the removal of the H2A.Z histone variant from nucleosomes through the NC2-INO80 complex, further enhancing chromatin accessibility at the *cat-3* promoter and TSS. VIB-1 works synergistically with CPC-1/GCN4 and NGF-1/GCN5-mediated histone H3 acetylation to facilitate efficient transcription factor binding. Together, these activities enable VIB-1 to dynamically regulate *cat-3* expression by recruiting transcriptional machinery, modulating chromatin structure, and cooperating with other transcriptional regulators, thereby ensuring an effective response to oxidative stress (Fig. 8D).

The Ndt80 domain has the most extensive DNA-binding interface among p53 superfamily members, with secondary structural elements that increase DNA-binding affinity, thereby enabling high-affinity binding of monomer Ndt80 proteins to target DNA [50, 52, 53]. Similarly, VIB-1 recognizes specific DNA motifs, such as the *cat-3* promoter, and mutations in key residues (R190A, R191A, R290A, and R291A) disrupt its DNA-binding ability and transcriptional activation of *cat-3*. Deletion of the DNA-binding domain reduces VIB-1 stability and impairs its function, while overexpression of a DNA-binding-deficient VIB-1 does not affect *cat-3* expression or H_2O_2 sensitivity in the WT strain, suggesting that intact DNA-binding activity is essential. These findings support the hypothesis that VIB-1 may function as a monomer to bind DNA and activate *cat-3* expression.

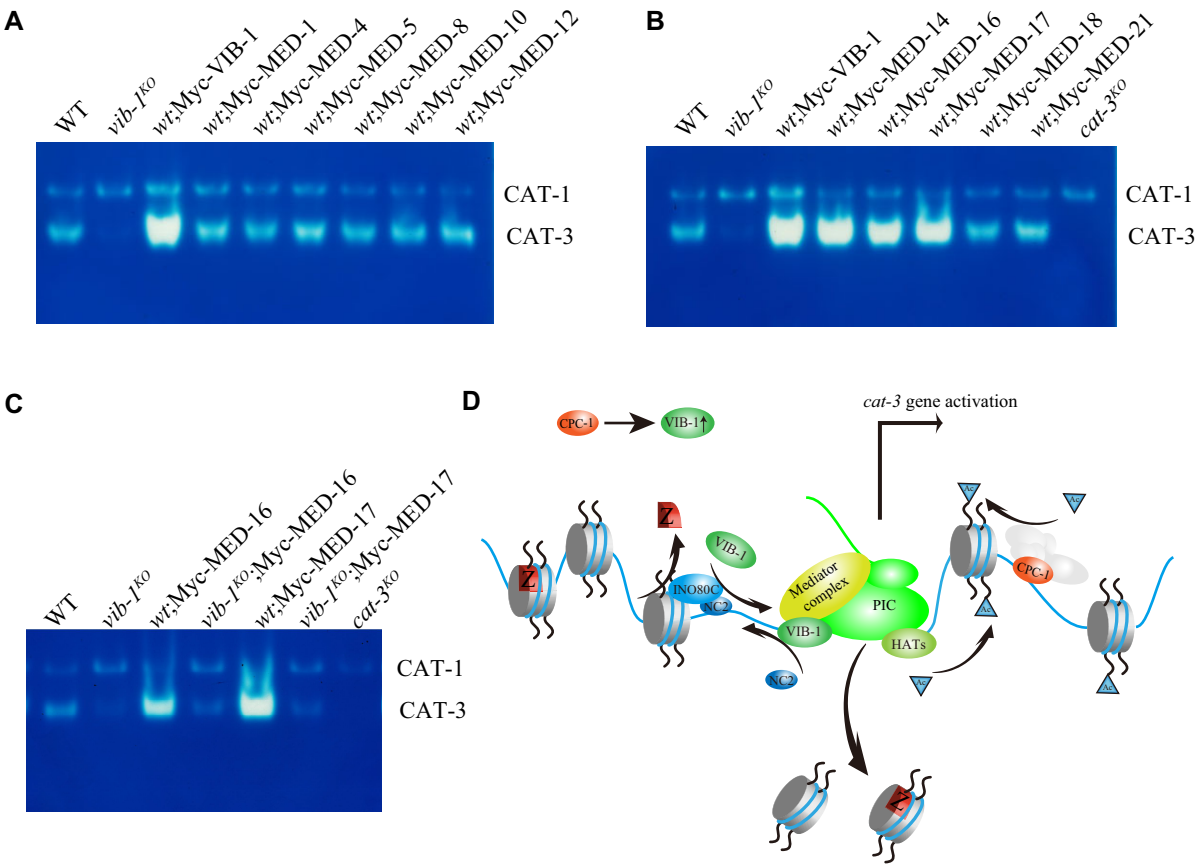

Figure 8. Overexpression of Mediator subunits increases CAT-3 levels, but requires VIB-1. (**A**–**C**) In-gel assay analysis of the CAT-3 activity levels in WT, *vib-1*^{KO}, *wt*;Myc-VIB-1 and Mediator subunits transformants strains. (**D**) A model depicting the mechanism of VIB-1 regulating *cat-3* expression. VIB-1 positively regulates *cat-3* expression in a dose-dependent manner by binding to the *cat-3* gene promoter via its DNA-binding domain. Specifically, VIB-1 interacts with GTFs and the Mediator complex for PIC assembly, which facilitate the removal of histone variant H2A.Z or the overall eviction of nucleosomes and promote histone acetylation. The NC2 complex activates *cat-3* gene expression by recruiting INO80C to remove H2A.Z from the *cat-3* promoter and by promoting VIB-1 recruitment. CPC-1 enhances *cat-3* expression by acetylating histones in the *cat-3* region and increasing VIB-1 levels. VIB-1 overexpression can bypass the need for CPC-1 and NC2 in *cat-3* activation.

Fungal responses to stress are intricate, specific, and multilayered, yet they rely on only a few evolutionarily conserved regulators. This suggests that a single regulator often coordinates multiple stress-specific responses [64, 65]. In *N. crassa*, VIB-1 serves as a prime example of such a regulator. VIB-1 is a multifunctional transcription factor that not only regulates catalase expression to lower intracellular ROS levels but also plays a role in HI and nutrient utilization [34, 35, 66]. This demonstrates *N. crassa*'s adaptive strategies to cope with complex environmental stress. Such integration of functions may relate to environmental adaptability, metabolic efficiency, and cellular protection mechanisms.

In fungi, HI processes are typically accompanied by ROS accumulation [67, 68], which, when excessive, can lead to PCD to kill the fused cells. ROS accumulation not only serves as a marker of stress, such as oxidative damage, but also functions as an intracellular signal triggering downstream process, including PCD [69–75]. During HI, ROS may act both as a signaling trigger and as an executor of cellular damage, with VIB-1 potentially playing a dual regulatory role in this context. From an evolutionary perspective, regulating oxidative stress and HI through a single transcription factor like VIB-1 may provide multiple adaptive advantages. First, such a mechanism could improve the efficiency of responses to environmental changes by utilizing shared signaling pathways. For example, when external stress increases ROS levels, VIB-1 can simultaneously activate antioxidant genes and initiate incompatibility responses to eliminate potential cellular threats. Second, employing a single regulator conserves genetic and metabolic resources, enhancing fungal competitiveness in resource-limited conditions.

Acknowledgements

We are very grateful to Mr. Yubo He for the crucial revision of this manuscript.

Author contributions: Conceptualization: H.L., Q.Z., X.L., and Q.H.; Data curation: H.L., X.L., and Q.H.; Formal analysis: H.L. and X.L.; Funding acquisition: Q.H. and X.L.; Investigation: H.L., Q.Z., F.H., and S.S.; Methodology: H.L., Q.Z., and S.S.; Project administration: H.L., Q.Z., and Q.H.; Resources: H.L., Q.Z., Q.H., and Y.W.; Software: H.L. and M.A.; Supervision: H.L.; Validation: H.L., Q.Z., F.H., and S.S.; Visualization: H.L., Q.Z., and F.H.; Writing—original draft: H.L., Q.Z., Q.H., Y.W., and M.A.; Writing—review & editing: H.L., Q.Z., X.L., Q.H., and M.A.

Supplementary data

Supplementary data is available at NAR online.

Conflict of interest

None declared.

Funding

This work was supported by National Key R&D Program of China [2018YFA0900500 to Q.H.] and 2115 Talent Development Program of China Agricultural University; Strategic Priority Research Program of the Chinese Academy of Sciences [XDA28030402, XDB0810000 to X.L.]. Funding to pay the Open Access publication charges for this article was provided by the National Key R&D Program of China [2018YFA0900500 to Q.H.]; Strategic Priority Research Program of the Chinese Academy of Sciences [XDA28030402, XDB0810000 to X.L.].

Data availability

All relevant data are within the manuscript and its Supplementary Data files.

References

1. Sies H, Jones DP. Reactive oxygen species (ROS) as pleiotropic physiological signalling agents. *Nat Rev Mol Cell Biol* 2020;**21**:363–83. https://doi.org/10.1038/s41580-020-0230-3
2. Zhang L, Wang X, Cueto R *et al.* Biochemical basis and metabolic interplay of redox regulation. *Redox Biol* 2019;**26**:101284. https://doi.org/10.1016/j.redox.2019.101284
3. Collin F. Chemical basis of reactive oxygen species reactivity and involvement in neurodegenerative diseases. *Int J Mol Sci* 2019;**20**:2407. https://doi.org/10.3390/ijms20102407
4. Cooke MS, Evans MD, Dizdaroglu M *et al.* Oxidative DNA damage: mechanisms, mutation, and disease. *FASEB j* 2003;**17**:1195–214. https://doi.org/10.1096/fj.02-0752rev
5. Rosca MG, Vazquez EJ, Chen Q *et al.* Oxidation of fatty acids is the source of increased mitochondrial reactive oxygen species production in kidney cortical tubules in early diabetes. *Diabetes* 2012;**61**:2074–83. https://doi.org/10.2337/db11-1437
6. Berlett BS, Stadtman ER. Protein oxidation in aging, disease, and oxidative stress. *J Biol Chem* 1997;**272**:20313–6. https://doi.org/10.1074/jbc.272.33.20313
7. Blokhina O, Virolainen E, Fagerstedt KV. Antioxidants, oxidative damage and oxygen deprivation stress: a review. *Ann Bot* 2003;**91**:179–94. https://doi.org/10.1093/aob/mcf118
8. Scandalios JG. Oxidative stress: molecular perception and transduction of signals triggering antioxidant gene defenses. *Braz J Med Biol Res* 2005;**38**:995–1014. https://doi.org/10.1590/S0100-879X2005000700003
9. Glorieux C, Zamocky M, Sandoval JM *et al.* Regulation of catalase expression in healthy and cancerous cells. *Free radic Biol Med* 2015;**87**:84–97.
10. Bigarella CL, Liang R, Ghaffari S. Stem cells and the impact of ROS signaling. *Development* 2014;**141**:4206–18. https://doi.org/10.1242/dev.107086
11. Mittler R. ROS are good. *Trends Plant Sci* 2017;**22**:11–9. https://doi.org/10.1016/j.tplants.2016.08.002
12. Michán S, Lledías F, Baldwin JD *et al.* Regulation and oxidation of two large monofunctional catalases. *Free Radical Biol Med* 2002;**33**:521–32. https://doi.org/10.1016/S0891-5849(02)00909-7
13. Schliebs W, Würtz C, Kunau WH *et al.* A eukaryote without catalase-containing microbodies: neurospora crassa exhibits a unique cellular distribution of its four catalases. *Euk Cell* 2006;**5**:1490–502. https://doi.org/10.1128/EC.00113-06
14. Michan S, Lledias F, Hansberg W. Asexual development is increased in neurospora crassa cat-3-null mutant strains. *Euk Cell* 2003;**2**:798–808. https://doi.org/10.1128/EC.2.4.798-808.2003
15. Qi S, He L, Zhang Q *et al.* Cross-pathway control gene CPC1/GCN4 coordinates with histone acetyltransferase GCN5 to regulate catalase-3 expression under oxidative stress in *Neurospora crassa*. *Free Radical Biol Med* 2018;**117**:218–27.
16. Dong Q, Wang Y, Qi S *et al.* Histone variant H2A.Z antagonizes the positive effect of the transcriptional activator CPC1 to regulate catalase-3 expression under normal and oxidative stress conditions. *Free Radical Biol Med* 2018;**121**:136–48.
17. Cui G, Dong Q, Duan J *et al.* NC2 complex is a key factor for the activation of catalase-3 transcription by regulating H2A.Z deposition. *Nucleic Acids Res* 2020;**48**:8332–48. https://doi.org/10.1093/nar/gkaa552
18. Zhou Y, Shen S, Du C *et al.* A role for the mitotic proteins Bub3 and BuGZ in transcriptional regulation of catalase-3 expression. *PLoS Genet* 2022;**18**:e1010254. https://doi.org/10.1371/journal.pgen.1010254
19. He L, Duan Z, Yu M *et al.* HDA-2-containing complex is required for activation of catalase-3 expression in neurospora crassa. *mBio* 2022;**13**:e0135122. https://doi.org/10.1128/mbio.01351-22
20. Chen CG, Yang YL, Shih HI *et al.* CaNdt80 is involved in drug resistance in *Candida albicans* by regulating CDR1. *Antimicrob Agents Chemother* 2004;**48**:4505–12. https://doi.org/10.1128/AAC.48.12.4505-4512.2004
21. Chen CG, Yang YL, Tseng KY *et al.* Rep1p negatively regulating MDR1 efflux pump involved in drug resistance in *Candida albicans*. *Fung Genet Biol* 2009;**46**:714–20. https://doi.org/10.1016/j.fgb.2009.06.003
22. Kappel L, Gaderer R, Flipphi M *et al.* The N-acetylglucosamine catabolic gene cluster in *Trichoderma reesei* is controlled by the Ndt80-like transcription factor RON1. *Mol Microbiol* 2016;**99**:640–57.https://doi.org/10.1111/mmi.13256
23. Hutchison EA, Glass NL. Meiotic regulators Ndt80 and ime2 have different roles in saccharomyces and neurospora. *Genetics* 2010;**185**:1271–82. https://doi.org/10.1534/genetics.110.117184
24. Doyle CE, Kitty Cheung HY, Spence KL *et al.* Unh1, an Ustilago maydis Ndt80-like protein, controls completion of tumor maturation, teliospore development, and meiosis. *Fung Genet Biol* 2016;**94**:54–68. https://doi.org/10.1016/j.fgb.2016.07.006
25. Shemesh E, Hanf B, Hagag S *et al.* Phenotypic and proteomic analysis of the *Aspergillus fumigatus* ΔPrtT, ΔXprG and ΔXprG/ΔPrtT protease-deficient mutants. *Front Microbiol* 2017;**8**:2490. https://doi.org/10.3389/fmicb.2017.02490
26. Hutchison EA, Bueche JA, Glass NL. Diversification of a protein kinase cascade: IME-2 is involved in nonself recognition and programmed cell death in *Neurospora crassa*. *Genetics* 2012;**192**:467–82. https://doi.org/10.1534/genetics.112.142612
27. Katz ME, Buckland R, Hunter CC *et al.* Distinct roles for the p53-like transcription factor XprG and autophagy genes in the response to starvation. *Fung Genet Biol* 2015;**83**:10–8. https://doi.org/10.1016/j.fgb.2015.08.006
28. Katz ME. Nutrient sensing-the key to fungal p53-like transcription factors? *Fung Genet Biol* 2019;**124**:8–16. https://doi.org/10.1016/j.fgb.2018.12.007
29. Xiang Q, Glass NL. Identification of vib-1, a locus involved in vegetative incompatibility mediated by het-c in *Neurospora crassa*. *Genetics* 2002;**162**:89–101. https://doi.org/10.1093/genetics/162.1.89
30. Xiang Q, Glass NL. The control of mating type heterokaryon incompatibility by vib-1, a locus involved in het-c heterokaryon incompatibility in *Neurospora crassa*. *Fungal Genetics Biol* 2004;**41**:1063–76.
31. Xu L, Ajimura M, Padmore R *et al.* NDT80, a meiosis-specific gene required for exit from pachytene in *Saccharomyces cerevisiae*. *Mol Cell Biol* 1995;**15**:6572–81. https://doi.org/10.1128/MCB.15.12.6572
32. Winter E. The Sum1/Ndt80 transcriptional switch and commitment to meiosis in *Saccharomyces cerevisiae*. *Microbiol*

Mol Biol Rev 2012;**76**:1–15. https://doi.org/10.1128/MMBR.05010-11
33. Dementhon K, Iyer G, Glass NL. VIB-1 is required for expression of genes necessary for programmed cell death in *Neurospora crassa*. *Euk Cell* 2006;**5**:2161–73. https://doi.org/10.1128/EC.00253-06
34. Xiong Y, Sun J, Glass NL. VIB1, a link between glucose signaling and carbon catabolite repression, is essential for plant cell wall degradation by *Neurospora crassa*. *PLoS Genet* 2014;**10**:e1004500. https://doi.org/10.1371/journal.pgen.1004500
35. Wu VW, Thieme N, Huberman LB *et al.* The regulatory and transcriptional landscape associated with carbon utilization in a filamentous fungus. *Proc Natl Acad Sci USA* 2020;**117**:6003–13. https://doi.org/10.1073/pnas.1915611117
36. Roca MG, Weichert M, Siegmund U *et al.* Germling fusion via conidial anastomosis tubes in the grey mould botrytis cinerea requires NADPH oxidase activity. *Fungal Biol* 2012;**116**:379–87. https://doi.org/10.1016/j.funbio.2011.12.007
37. Ishikawa FH, Souza EA, Read ND *et al.* Live-cell imaging of conidial fusion in the bean pathogen, colletotrichum lindemuthianum. *Fungal Biol* 2010;**114**:2–9. https://doi.org/10.1016/j.funbio.2009.11.006
38. Fischer-Harman V, Jackson KJ, Muñoz A *et al.* Evidence for tryptophan being a signal molecule that inhibits conidial anastomosis tube fusion during colony initiation in *Neurospora crassa*. *Fung Genet Biol* 2012;**49**:896–902. https://doi.org/10.1016/j.fgb.2012.08.004
39. Belden WJ, Larrondo LF, Froehlich AC *et al.* The band mutation in *Neurospora crassa* is a dominant allele of ras-1 implicating RAS signaling in circadian output. *Genes Dev* 2007;**21**:1494–505. https://doi.org/10.1101/gad.1551707
40. He Q, Cha J, He Q *et al.* CKI and CKII mediate the frequency-dependent phosphorylation of the white collar complex to close the Neurospora circadian negative feedback loop. *Genes Dev* 2006;**20**:2552–65. https://doi.org/10.1101/gad.1463506
41. Wang Y, Dong Q, Ding Z *et al.* Regulation of neurospora catalase-3 by global heterochromatin formation and its proximal heterochromatin region. *Free Radical Biol Med* 2016;**99**:139–52.
42. Shen S, Zhang C, Meng Y *et al.* Sensing of H2O2-induced oxidative stress by the UPF factor complex is crucial for activation of catalase-3 expression in Neurospora. *PLoS Genet* 2023;**19**:e1010985. https://doi.org/10.1371/journal.pgen.1010985
43. He L, Guo W, Li J *et al.* Two dominant selectable markers for genetic manipulation in *Neurospora crassa*. *Curr Genet* 2020;**66**:835–47. https://doi.org/10.1007/s00294-020-01063-1
44. Zhao Y, Shen Y, Yang S *et al.* Ubiquitin ligase components Cullin4 and DDB1 are essential for DNA methylation in *Neurospora crassa*. *J Biol Chem* 2010;**285**:4355–65. https://doi.org/10.1074/jbc.M109.034710
45. Lledías F, Rangel P, Hansberg W. Oxidation of catalase by singlet oxygen. *J Biol Chem* 1998;**273**:10630–7. https://doi.org/10.1074/jbc.273.17.10630
46. Livak KJ, Schmittgen TD. Analysis of relative gene expression data using real-time quantitative PCR and the 2 (-Delta Delta C (T)) method. *Methods* 2001;**25**:402–8. https://doi.org/10.1006/meth.2001.1262
47. Zhou Z, Liu X, Hu Q *et al.* 2013; Suppression of WC-independent frequency transcription by RCO-1 is essential for Neurospora circadian clock. *Proc Natl Acad Sci USA*, **110**:E4867–74.
48. Gai K, Cao X, Dong Q *et al.* Transcriptional repression of frequency by the IEC-1-INO80 complex is required for normal Neurospora circadian clock function. *PLoS Genet* 2017;**13**:e1006732. https://doi.org/10.1371/journal.pgen.1006732
49. Duan J, Liu Q, Su S *et al.* The neurospora RNA polymerase II kinase CTK negatively regulates catalase expression in a chromatin context-dependent manner. *Environ Microbiol* 2020;**22**:76–90. https://doi.org/10.1111/1462-2920.14821
50. Lamoureux JS, Glover JN. Principles of protein–DNA recognition revealed in the structural analysis of Ndt80-MSE DNA complexes. *Structure* 2006;**14**:555–65. https://doi.org/10.1016/j.str.2005.11.017
51. Lamoureux JS, Stuart D, Tsang R *et al.* Structure of the sporulation-specific transcription factor Ndt80 bound to DNA. *EMBO J* 2002;**21**:5721–32. https://doi.org/10.1093/emboj/cdf572
52. Fingerman IM, Sutphen K, Montano SP *et al.* Characterization of critical interactions between Ndt80 and MSE DNA defining a novel family of ig-fold transcription factors. *Nucleic Acids Res* 2004;**32**:2947–56. https://doi.org/10.1093/nar/gkh625
53. Montano SP, Coté ML, Fingerman I *et al.* Crystal structure of the DNA-binding domain from Ndt80, a transcriptional activator required for meiosis in yeast. *Proc Natl Acad Sci USA* 2002;**99**:14041–6. https://doi.org/10.1073/pnas.222312199
54. Paluh JL, Plamann M, Krüger D *et al.* Determination of the inactivating alterations in two mutant alleles of the *Neurospora crassa* cross-pathway control gene cpc-1. *Genetics* 1990;**124**:599–606. https://doi.org/10.1093/genetics/124.3.599
55. Dong Q, Wang Y, Qi S *et al.* Histone variant H2A.Z antagonizes the positive effect of the transcriptional activator CPC1 to regulate catalase-3 expression under normal and oxidative stress conditions. *Free Radical Biol Med* 2018;**121**:136–48. https://doi.org/10.1016/j.freeradbiomed.2018.05.003
56. Goppelt A, Stelzer G, Lottspeich F *et al.* A mechanism for repression of class II gene transcription through specific binding of NC2 to TBP-promoter complexes via heterodimeric histone fold domains. *EMBO J* 1996;**15**:3105–16. https://doi.org/10.1002/j.1460-2075.1996.tb00673.x
57. Goppelt A, Meisterernst M. Characterization of the basal inhibitor of class II transcription NC2 from *Saccharomyces cerevisiae*. *Nucleic Acids Res* 1996;**24**:4450–5. https://doi.org/10.1093/nar/24.22.4450
58. Prelich G. *Saccharomyces cerevisiae* BUR6 encodes a DRAP1/NC2alpha homolog that has both positive and negative roles in transcription *in vivo*. *Mol Cell Biol* 1997;**17**:2057–65. https://doi.org/10.1128/MCB.17.4.2057
59. Inostroza JA, Mermelstein FH, Ha I *et al.* Dr1, a TATA-binding protein-associated phosphoprotein and inhibitor of class II gene transcription. *Cell* 1992;**70**:477–89. https://doi.org/10.1016/0092-8674(92)90172-9
60. Meisterernst M, Roeder RG. Family of proteins that interact with TFIID and regulate promoter activity. *Cell* 1991;**67**:557–67. https://doi.org/10.1016/0092-8674(91)90530-C
61. Smith CA, Bates P, Rivera-Gonzalez R *et al.* ICP4, the major transcriptional regulatory protein of herpes simplex virus type 1, forms a tripartite complex with TATA-binding protein and TFIIB. *J Virol* 1993;**67**:4676–87. https://doi.org/10.1128/jvi.67.8.4676-4687.1993
62. Grondin B, DeLuca N. Herpes simplex virus type 1 ICP4 promotes transcription preinitiation complex formation by enhancing the binding of TFIID to DNA. *J Virol* 2000;**74**:11504–10. https://doi.org/10.1128/JVI.74.24.11504-11510.2000
63. Lester JT, DeLuca NA. Herpes simplex virus 1 ICP4 forms complexes with TFIID and mediator in virus-infected cells. *J Virol* 2011;**85**:5733–44. https://doi.org/10.1128/JVI.00385-11
64. Yaakoub H, Mina S, Calenda A *et al.* Oxidative stress response pathways in fungi. *Cell Mol Life Sci* 2022;**79**:333. https://doi.org/10.1007/s00018-022-04353-8
65. Hagiwara D, Sakamoto K, Abe K *et al.* Signaling pathways for stress responses and adaptation in Aspergillus species: stress biology in the post-genomic era. *Biosci Biotechnol Biochem* 2016;**80**:1667–80. https://doi.org/10.1080/09168451.2016.1162085
66. Xiang Q, Glass NL. The control of mating type heterokaryon incompatibility by vib-1, a locus involved in het-c heterokaryon incompatibility in *Neurospora crassa*. *Fung Genet Biol* 2004;**41**:1063–76. https://doi.org/10.1016/j.fgb.2004.07.006
67. Lu C, Katayama T, Mori N *et al.* Mitochondrial fission dysfunction alleviates heterokaryon incompatibility-triggered cell death in the industrial filamentous fungus *Aspergillus oryzae*.

bioRxiv, https://doi.org/10.1101/2021.12.10.472196, 11 October 2021, preprint: not peer reviewed.
68. Hutchison E, Brown S, Tian C *et al.* Transcriptional profiling and functional analysis of heterokaryon incompatibility in *Neurospora crassa* reveals that reactive oxygen species, but not metacaspases, are associated with programmed cell death. *Microbiology* 2009;**155**:3957–70. https://doi.org/10.1099/mic.0.032284-0
69. Cano-Domínguez N, Alvarez-Delfín K, Hansberg W *et al.* NADPH oxidases NOX-1 and NOX-2 require the regulatory subunit NOR-1 to control cell differentiation and growth in *Neurospora crassa*. *Euk Cell* 2008;**7**:1352–61. https://doi.org/10.1128/EC.00137-08
70. Dickinson BC, Chang CJ. Chemistry and biology of reactive oxygen species in signaling or stress responses. *Nat Chem Biol* 2011;**7**:504–11. https://doi.org/10.1038/nchembio.607
71. Dickinson BC, Peltier J, Stone D *et al.* Nox2 redox signaling maintains essential cell populations in the brain. *Nat Chem Biol* 2011;**7**:106–12. https://doi.org/10.1038/nchembio.497
72. Lara-Ortíz T, Riveros-Rosas H, Aguirre J. Reactive oxygen species generated by microbial NADPH oxidase NoxA regulate sexual development in *Aspergillus nidulans*. *Mol Microbiol* 2003;**50**:1241–55. https://doi.org/10.1046/j.1365-2958.2003.03800.x
73. Rajendran P, Nandakumar N, Rengarajan T *et al.* Antioxidants and human diseases. *Clin Chim Acta* 2014;**436**:332–47. https://doi.org/10.1016/j.cca.2014.06.004
74. Locato V, Paradiso A, Sabetta W *et al.* In: Wendehenne D (ed.), *Adv Bot Res*. Vol. **77**, London, UK: Academic Press, 2016, 165–92.
75. Ye C, Zheng S, Jiang D *et al.* Initiation and execution of programmed cell death and regulation of reactive oxygen species in plants. *Int J Mol Sci* 2021;**22**:12942. https://doi.org/10.3390/ijms222312942

Received: September 3, 2024. **Revised:** February 7, 2025. **Editorial Decision:** February 20, 2025. **Accepted:** February 22, 2025